frontiers in Earth Science

ORIGINAL RESEARCH
published: 13 December 2021
doi: 10.3389/feart.2021.760100

Mesozoic–Cenozoic Uplift/Exhumation History of the Qilian Shan, NE Tibetan Plateau: Constraints From Low-Temperature Thermochronology

Lihao Chen[1], Chunhui Song[1], Yadong Wang[2,3], Xiaomin Fang[2,4], Yihu Zhang[1], Jing Zhang[1], Yongfa Chen[1] and Pengju He[1]*

[1]School of Earth Sciences and Key Laboratory of Mineral Resources in Western China (Gansu Province), Lanzhou University, Lanzhou, China, [2]Northwest Institute of Eco-Environment and Resources, Chinese Academy of Sciences and Key Laboratory of Petroleum Resources, Gansu Province, Lanzhou, China, [3]Rock-Mineral Preparation and Fission Track Dating Laboratory of Geochemical Analysis and Testing Center, Northwest Institute of Eco-Environment and Resources, Chinese Academy of Sciences (CAS), Lanzhou, China, [4]Key Laboratory of Continental Collision and Plateau Uplift, Institute of Tibetan Plateau Research, Chinese Academy of Sciences, Beijing, China

OPEN ACCESS

Edited by:
Tara N. Jonell,
University of Glasgow,
United Kingdom

Reviewed by:
Andrew V. Zuza,
University of Nevada, Reno,
United States
Xing Jian,
Xiamen University, China
Bangshen Qi,
Chinese Academy of Geological Sciences, China

***Correspondence:**
Chunhui Song
songchh@lzu.edu.cn

Specialty section:
This article was submitted to Quaternary Science, Geomorphology, and Paleoenvironment, a section of the journal Frontiers in Earth Science

Received: *17 August 2021*
Accepted: *26 October 2021*
Published: *13 December 2021*

Citation:
Chen L, Song C, Wang Y, Fang X, Zhang Y, Zhang J, Chen Y and He P (2021) Mesozoic–Cenozoic Uplift/Exhumation History of the Qilian Shan, NE Tibetan Plateau: Constraints From Low-Temperature Thermochronology. Front. Earth Sci. 9:760100. doi: 10.3389/feart.2021.760100

The Qilian Shan, which is located along the northeastern margin of the Tibetan Plateau, plays a key role in understanding the dynamics of the outward and upward growth of the plateau. However, when and how tectonic deformation evolved into the geographic pattern which is currently observed in the Qilian Shan are still ambiguous. Here, apatite fission track (AFT) thermochronology and sedimentology were conducted to interpret the low-temperature tectonic deformation/exhumation events in well-dated Late Miocene synorogenic sediment sequences in the Xining Basin, which is adjacent to the southern flank of the Qilian Shan. These new low-temperature thermochronological results suggest that the Qilian Shan experienced four stages of tectonic exhumation during the late Mesozoic–Cenozoic. The Late Cretaceous exhumation events in the Qilian Shan were caused by the diachronous Mesozoic convergence of the Asian Plate and Lhasa Block. In the early Cenozoic (ca. 68–48 Ma), the Qilian Shan quasi-synchronously responded to the Indian–Asian plate collision. Subsequently, the mountain range experienced a two-phase deformation during the Eocene–Early Miocene due to the distal effects of ongoing India–Asia plate convergence. At ca. 8 ± 1 Ma, the Qilian Shan underwent dramatic geomorphological deformation, which marked a change in subsidence along the northeastern margin of the Tibetan Plateau at that time. Our findings suggest that the paleogeographic pattern in the northeastern Tibetan Plateau was affected by the pervasive suture zones in the entire Qilian Shan, in which the pre-Cenozoic and Indian–Asian plate motions reactivated the transpressional faults which strongly modulated the multiperiodic tectonic deformation in northern Tibet during the Cenozoic. These observations provide new evidence for understanding the dynamic mechanisms of the uplift and expansion of the Tibetan Plateau.

Keywords: Apatite fission track, Northern Tibetan Plateau, Xining Basin, Qilian Shan, Tectonic exhumation, Geomorphological, NE Tibetan Plateau

INTRODUCTION

With continuous Cenozoic compression and convergence between the Indian and Asian plates, the uplift and expansion of the Tibetan Plateau has profoundly influenced the climatic and paleogeographical evolution in Asia (England and Houseman, 1986; Harrison et al., 1992; Dupont-Nivet et al., 2008; Fang et al., 2019; Spicer et al., 2020). Several tectonic geodynamic evolution models present different interpretations of the topographic spatial–temporal deformation mechanism of the Tibetan Plateau. For example, some studies suggest that growth on the northeastern margin of the plateau was driven by continuous lithospheric shortening and monotonic deformation induced by propagation of stresses from south to north during the Pliocene–Quaternary (Meyer et al., 1998; Tapponnier et al., 1990; Tapponnier et al., 2001; Hu et al., 2019). However, recent deforming mantle models suggest that the deformation initiated quasi-synchronously in the early Cenozoic throughout the whole Tibetan Plateau (for example, Yin and Harrison, 2000; Yin et al., 2008; Dayem et al., 2009; Clark, 2012; Clark et al., 2010). The northeastern margin of the plateau developed multiple orogenic belts, which significantly constrains the timing of the far-field effects of plate collision and the mechanism of plateau expansion (Tapponnier et al., 2001; Lease et al., 2012). The Qilian Shan trends in the northwest direction between the Alxa and Qaidam Blocks, which comprise the northeastern margin of the Tibetan Plateau (**Figure 1A**). As a frontier tectonic belt that formed in response to the plateau-related collision, the Qilian Shan is a key to test deformation events, and the growth model of the plateau edge has garnered significant attention. Recent studies have revealed the Cenozoic tectonic history of the Qilian Shan, but the initial timing of tectonism and the growth evolution of the mountain range have remained elusive. Two consensuses have emerged regarding the timing of prominent deformation in the Qilian Shan, namely, the early Cenozoic (Yin et al., 2002; Yin et al., 2008; He et al., 2017; He et al., 2020a; He et al., 2020b) and the late Cenozoic (Wang et al., 2017; Pang et al., 2019a; Wang et al., 2020), and these models yield distinctly different predictions of the mechanism of the plateau growth. Moreover, Cretaceous tectonic signals have also been found in the Qilian Shan (Jolivet et al., 2001; Qi et al., 2016; Li et al., 2019), but research regarding the Mesozoic tectonic evolution of the southern, central, and northern Qilian Shan is relatively scarce (Vincent and Allen 1999; Chen et al., 2002; Cheng et al., 2019).

The Xining Basin (XB) is adjacent to the convergence zone of the southern, central and northern Qilian orogenic belts (**Figure 1B**). This basin developed a thick and continuous late Cenozoic sediment sequence, and the depositional age of this sequence has been constrained by fine-scale paleomagnetism and mammalian fossil chronology (Yang et al., 2017; Zhang et al., 2017). Therefore, the XB is an ideal site to constrain the temporal evolution of basin–mountain coupling. Detrital apatite fission track (AFT) thermochronology research is a significant means to invert the tectonic evolution of orogenic belts and basin formation and to recover paleogeography during basin–mountain coupling (Bernet and Spiegel, 2004). Previous studies have provided large amounts of low-temperature thermochronological information on the sedimentary strata and nearby bedrock in the XB, but the interpretation of AFT ages of sediments deposited after the Late Miocene is still unclear (Wang et al., 2015b; Wang et al., 2016; Lease et al., 2011). In this study, we present detrital AFT and sedimentological evidence from two well-dated late Cenozoic synorogenic sections in the XB, which constrain the linkages to the Mesozoic–Cenozoic tectonic evolution of the Qilian Shan. Our observations provide further insight into the involvement of per-Cenozoic plate motions and the Cenozoic multiepisodic tectonic exhumation history of the Qilian Shan. Although the timing of the initial Indian–Asian plate collision remains controversial, most current studies suggest that the plates initially collided at approximately 55 ± 10 Ma (Najman et al., 2010; Ding et al., 2017). Notably, no extensive Cenozoic volcanic activity occurred near the XB, from which it can be deduced that the exhumation/cooling events in this study of the Qilian Shan were caused by tectonically driven local terrain deformation rather than by magmatic cooling and eruption (Gansu Geologic Bureau, 1989; Gehrels et al., 2003; He et al., 2020a). Hence, the early Cenozoic cooling signals indicate that the Qilian Shan quasi-synchronously responded to the Indian–Asian plate collision, which is also consistent with previous research in other parts of the northeastern margin of the Tibetan Plateau (Dupont-Nivetet et al., 2004; Dai et al., 2005; Jian et al., 2013; Jian et al., 2018; Fan et al., 2019; Cheng et al., 2019; Fang et al., 2019; Hong et al., 2020). These results enrich the knowledge of the Late Cretaceous–Cenozoic paleogeomorphological growth history of the northeastern Plateau.

GEOLOGICAL SETTING

The Qilian Shan is located in the northernmost portion of the Tibetan Plateau and is divided into multiple basin–mountain units by a series of subparallel NW-SE striking thrusts, folds, and strike-slip faults (Meyer et al., 1998) (**Figure 1B**). The main basins around the Qilian Shan, including the Qaidam Basin, Hexi Corridor Basin, and XB, have thick and extensive Cenozoic sediments (**Figure 1B**). The XB is adjacent to the eastern part of the Qilian Shan and is in the transition zone between the Tibetan Plateau and the Loess Plateau. This NW-oriented quadrilateral inland Cenozoic basin is related to a dome structure composed of Proterozoic, early Proterozoic, and Mesoproterozoic orogenic belts (Fang et al., 2019). The basin is bound by the Laji Shan, Daban Shan, and Riyueshan faults to the south, north, and west, respectively (QBGM, 1991). The mountains around the basin are situated in the Central Qilian orogenic belt, in which the Huangshui River cuts through the Cenozoic strata providing good natural sections for researchers to trace the tectonism history of the Qilian Shan and the adjacent basins on the northeastern margin of the Tibetan Plateau. Previous studies on the tectonic history of the northeastern Tibetan Plateau have obtained a series of important achievements (Meyer et al., 1998; Tapponnier et al., 2001; Yin et al., 2002; Yin et al., 2008; Lease et al., 2011; Jian et al., 2013; Yuan et al., 2013; Allen et al., 2017; Jian et al., 2018; Fang et al.,

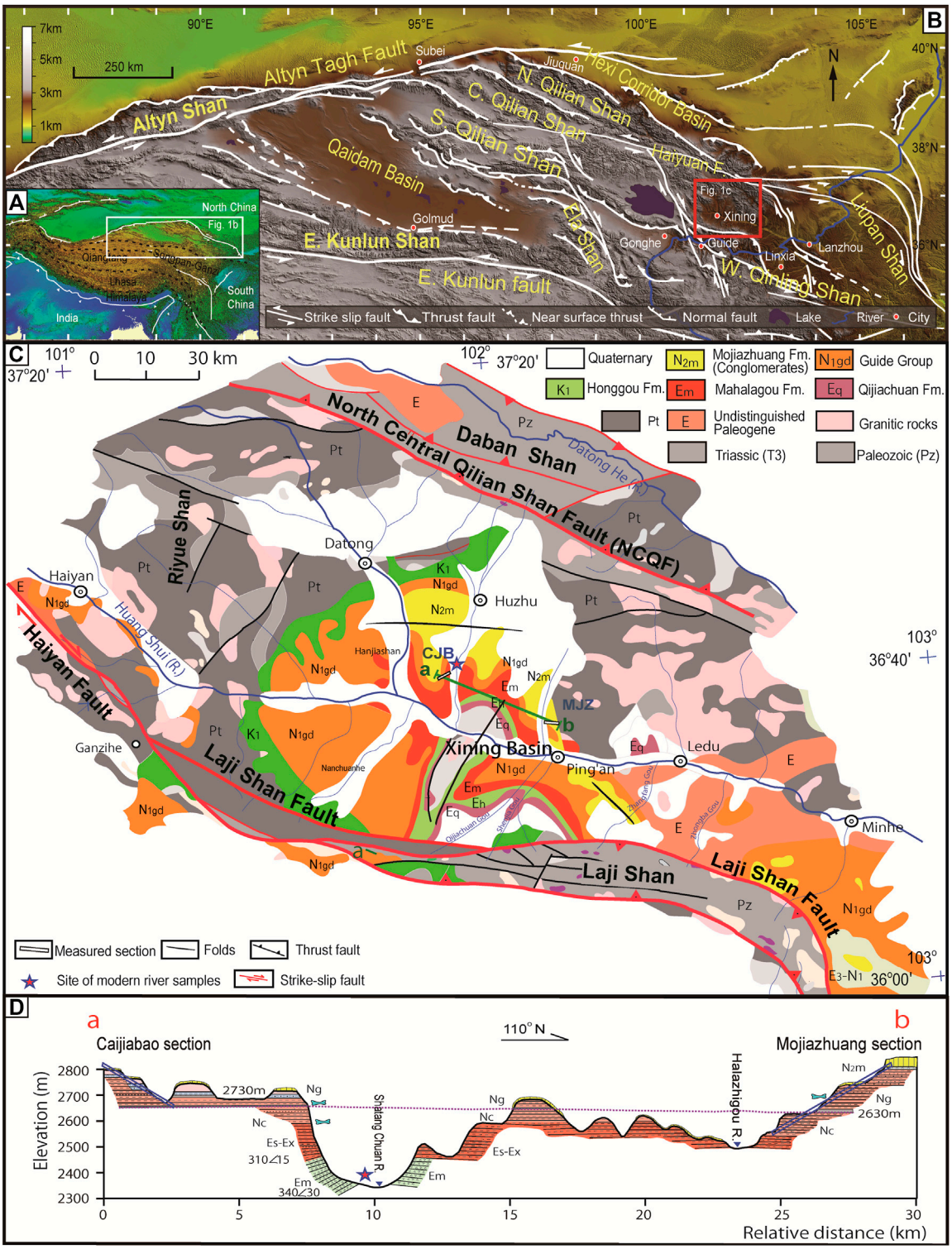

FIGURE 1 | Geologic survey of the study area on the Tibetan Plateau. **(A)** Digital topographic elevation model of the northeastern Tibetan Plateau mainly indicates the location of the Qilian Shan geomorphology and adjacent basins. **(B)** Topography of the major faults in the TP and Qilian Shan in the northeastern region and the periphery. **(C)** Distribution of the Cenozoic stratigraphy of the XB and locations of the CJB (Caojiabao) and MJZ (Mojiazhuang) sections (modified from Dai et al., 2005). **(D)** Sections a–b show the relationships between the Cenozoic stratigraphy and the CJB and MJZ sections for the top sequences (modified from Zhang et al., 2017).

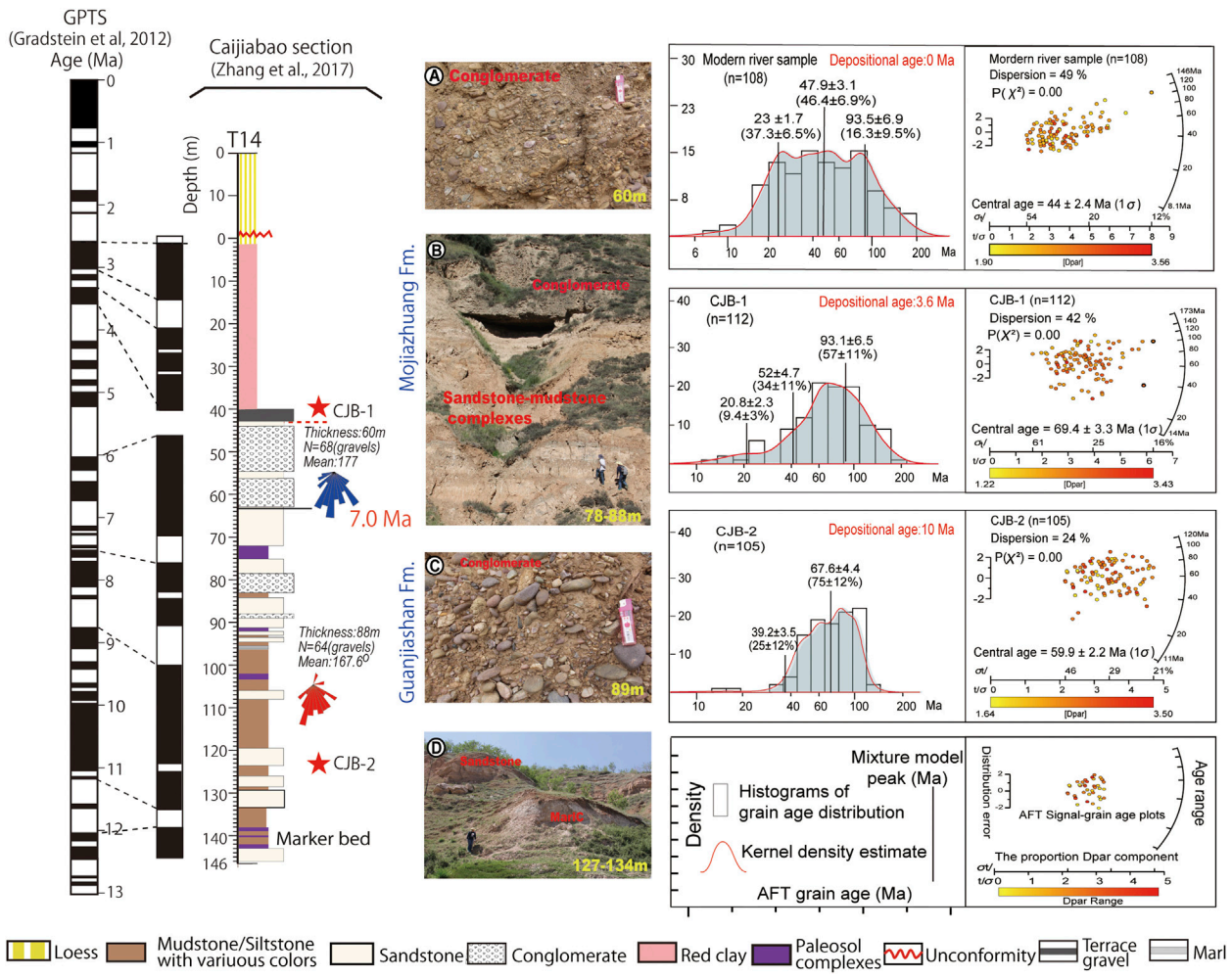

FIGURE 2 | Magnetostratigraphy, stratigraphic column, paleocurrent directions (from Zhang et al., 2017 except the new data marked by red arrows), sampling sites, and low-temperature thermochronology results for the Caojiabao (CJB) section. **(A–D)** Photographs showing the representative stratigraphy for the section. The detrital AFT grain ages of CJB-1, CJB-2, and modern river samples were statistically decomposed into components (with modeled component peak ages and proportions) and chi-square tests through RadialPlotter and DensityPlotter (Vermeesch, 2012).

2019; Hong et al., 2020; Cheng et al., 2021). Current sedimentological and low-temperature thermochronological evidence suggests that the region quasi-synchronously responded to the Indian–Asian Plate collision during the early Cenozoic, and then it entered a period of relative quiescence (Duvall et al., 2013; Pan et al., 2013; Wang et al., 2016; Zhang et al., 2016; An et al., 2020). Subsequently, widespread faulting and orogenic belt deformation occurred at ~15 Ma (Zheng et al., 2017; Pang et al., 2019b; Yu et al., 2019). Along with the continued northward compression of the plateau and eastward propagation of the Haiyuan faults, the bedrock and basin sediments recorded many rapid exhumation/deposition events during 8–10 Ma (Fang et al., 2005; Zheng et al., 2010; Fang et al., 2012; Wang et al., 2016; Zhuang et al., 2018). The large amounts of low-temperature thermochronological data published in recent years show that the Qilian Shan has experienced four stages of cooling history: Late Triassic–Early Cretaceous (Jolivet et al., 2001; Qi et al., 2016); Late Cretaceous–Eocene (Jian et al., 2013; Li et al., 2013; Pan et al., 2013; Wang et al., 2016; Jian et al., 2018); Oligocene–Middle Miocene (Li et al., 2013; Yu et al., 2017) and Late Miocene (Zheng et al., 2017; Pang et al., 2019a; Wang et al., 2020). Most of the bedrock data focus on the Oligocene–Early Miocene and Late Miocene (Zheng et al., 2010; Zheng et al., 2017; Meng et al., 2020; Wang et al., 2020), while detrital data in the basin cover all the stages of cooling ages (Pan et al., 2013; He et al., 2017; He et al., 2018; He et al., 2020b).

In this study, we selected two Late Miocene–Pliocene sequences in the Caojiabao (CJB) (12.4–2.6 Ma) (36°42′55.8″ N, 101°49′42″ E; elevation: 2,740 m) and Mojiazhuang (MJZ) (12.7–4.8 Ma) (36°41′07.08″ N, 102°04′15.78″ E; Elevations: 2,840 m) sections within the XB and collected samples for detailed low-temperature thermochronological research. The CJB and MJZ sections are the uppermost sequences of the Cenozoic basin strata and are located at the center and

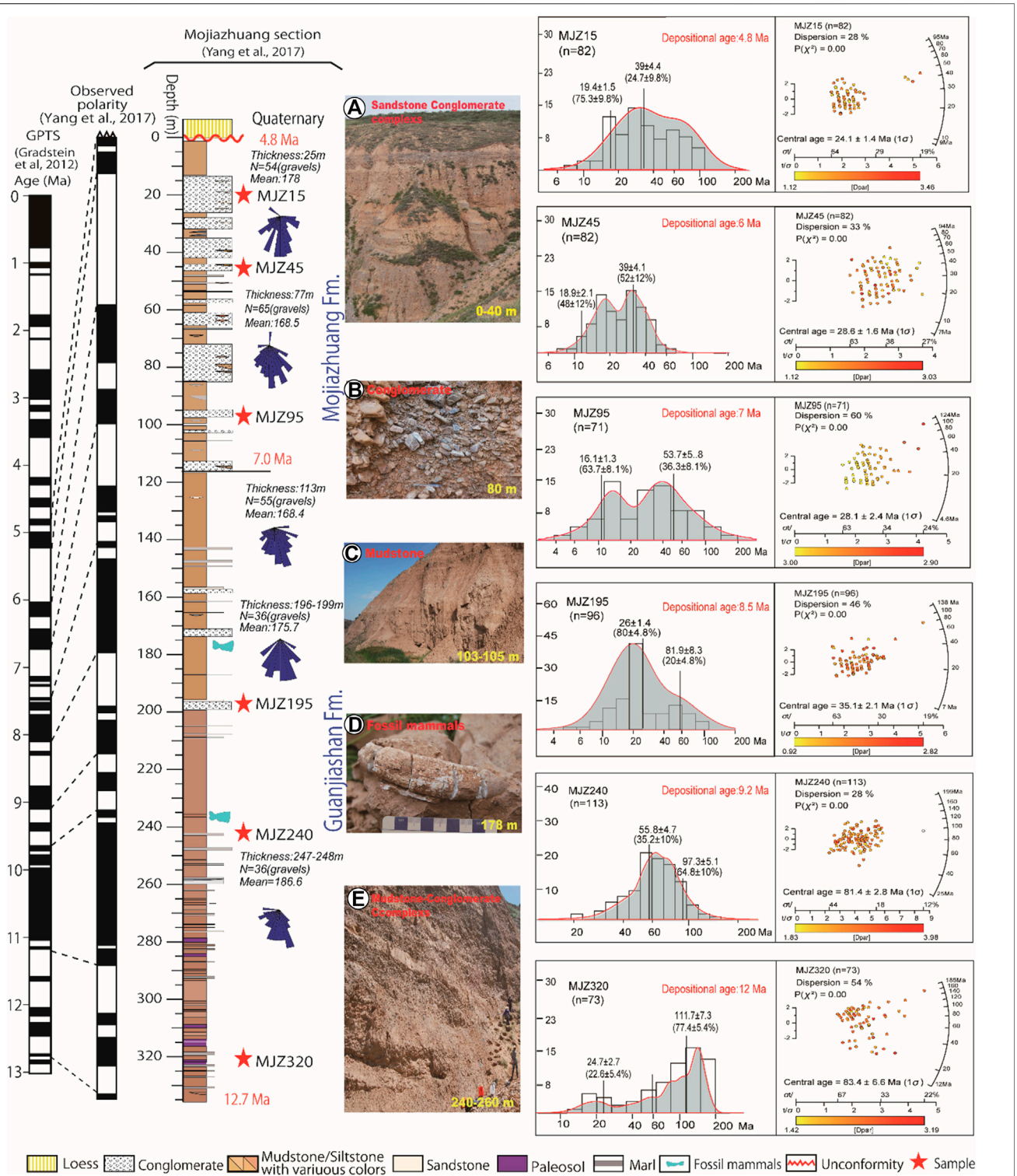

FIGURE 3 | Magnetostratigraphy, stratigraphic column, paleocurrent directions (all from Yang et al., 2017), sampling sites, and low-temperature thermochronology results for the Mojiazhuang (MJZ) section. The detrital AFT grain ages of the samples were statistically analyzed using RadialPlotter and DensityPlotter (Vermeesch, 2012). **(A–F)** Photographs of representative stratigraphy in the section.

TABLE 1 | Detrital AFT data from sediment samples.

Sample	*n*	Track density ($\times10^5$)			U (ppm)	*p* (χ^2)	Central age (Ma)	Average Dpar (range) (μm)	Mean track length ± SD (μm)	No. lengths
		Fossil (N_s) ($\times10^5$ cm^{-2})	Induced (N_i) ($\times10^5$ cm^{-2})	Dosimeter (N_d) ($\times10^6$ cm^{-2})						
Modern river sample	108	1.63 (2023)	8.28 (10,308)	1.68 (17,656)	7.43	0	44 ± 2.4	2.56 (1.9–3.56)	13.01 ± 1.52	60
CJB-1	112	2.04 (2,198)	5.86 (6,301)	1.37 (13,301)	6.6	0	69.4 ± 3.3	1.92 (1.22–3.43)	13.58 ± 1.62	80
MJZ15	82	1.69 (450)	16.14 (4,280)	1.45 (13,301)	14.93	0	24.1 ± 1.4	2.54 (1.12–3.46)	13.24 ± 1.62	72
MJZ45	82	2.3 (618)	16.32 (4,389)	1.44 (13,301)	16.32	0	28.6 ± 1.6	1.83 (1.12–3.03)	14.03 ± 1.54	61
MJZ95	71	1.6 (529)	14.65 (4,844)	1.42 (13,301)	14.45	0	28.1 ± 2.4	1.67 (1.03–2.74)	13.19 ± 1.42	53
MJZ195	96	1.88 (845)	11.13 (4,999)	1.43 (13,301)	11.5	0	25.5 ± 1.4	1.73 (0.92–2.82)	13.56 ± 1.18	54
MJZ240	113	3.85 (3,111)	8.8 (7,123)	1.41 (13,301)	9.06	0	81.4 ± 2.8	2.68 (1.83–3.98)	13.27 ± 1.24	51
CJB-2	105	1.18 (1702)	3.69 (5,311)	1.38 (13,301)	4.21	0	59.9 ± 2.7	2.54 (1.64–3.5)	13.95 ± 1.67	80
MJZ320	73	1.53 (664)	4.25 (1848)	1.42 (13,301)	4.62	0	83.4 ± 6.6	2.23 (1.42–3.19)	13.14 ± 1.74	46

Note: *ρs: spontaneous track densities measured in internal mineral surfaces; ρi and ρd: induced and dosimeter track densities on external mica detector; in bracket is the number of tracks and radiation flux; p(χ^2): probability of obtaining χ^2 value for single-grain ages degrees of freedom; Dpar is the fission tracks etch pit measurements.*

TABLE 2 | Detrital AFT peak-fitting data.

Sample	Depositional Age (Ma)	*n*	Age range (Ma)	P_1	P_2	P_3	P_4
Modern river sample	0	108	9.49–181	23 ± 1.7 37.3 ± 6.5%	—	47.9 ± 2.9 46.4 ± 6.9%	93.5 ± 6.9 16.3 ± 9.5%
CJB-1	3.6	118	13.52–173.08	20.8 ± 2.3 9.4 ± 3%	—	52 ± 4.7 34 ± 11%	93.1 ± 9.5 57 ± 11%
MJZ15	4.8	82	8.59–95	19.4 ± 1.5 75.3 ± 9.8%	39 ± 4.4 24.7 ± 9.8%	—	—
MJZ45	6	82	6.4–94	18.9 ± 2.1 48 ± 12%	39 ± 4.1 52 ± 12%	—	—
MJZ95	7	71	5.97–159.97	16.1 ± 1.3 63.7 ± 8.1%	—	53.7 ± 5.8 36.3 ± 8.1%	—
MJZ195	8.5	96	5.4–138	—	26 ± 1.4 80 ± 4.8%	—	81.9 ± 8.3 20 ± 4.8%
MJZ240	9.2	113	25.18–198.61	—	—	55.8 ± 4.7 35.2 ± 10%	97.3 ± 5.1 64.8 ± 10%
CJB-2	10	105	14.2–151.38	—	39.2 ± 3.5 25 ± 12%	67.6 ± 4.4 75 ± 12%	—
MJZ320	12	81	12.28–184.83	24.7 ± 2.7 22.6 ± 5.4%	—	—	111.7 ± 7.3 77.4 ± 5.4%

Note: *The binomial peak-fitting ages are given in 1 Ma ± 1 SE. The percentage of grains in a specific peak is also given.* N = *total number of analyzed grains; "—" is no data. The depositional ages of the XB are determined by magnetostratigraphy, and their errors are lower than 0.1 Ma. Sample single-grain ages are statistically decomposed into age components (P1–P4) by Density Plotter (Vermeesch, 2012). The modeled peak ages (with estimated standard deviations) and proportions of age components are given. Depositional ages of samples from the Mojiazhuang and Caojiabao sections are correlated to the magnetostratigraphic ages from Zhang et al. (2016) and Yang et al. (2017).*

northeast of the XB, respectively (Zhang et al., 2017; Yang et al., 2017; Fang et al., 2019) (**Figure 1C,D**). The strata exposed in these two sections are divided into the Guanjiashan Fm. (formerly the Xianshuihe Fm.) and Mojiazhuang Fm. from bottom to top according to regional stratigraphic correlation (**Figures 2**, **3**). Limited high-resolution magnetostratigraphy and *in situ* mammalian fossils indicate that the Guanjiashan Fm. is 140–64 m thick and 12–7 Ma in age in the CJB section and 336–137 m thick and 12.7–7 Ma in age in the MJZ section (Fang et al., 2019) (**Figures 2**, **3**). Based on the lithologic assemblage and mammalian fossils, the Guanjiashan Fm. is divided into two units (Yang et al., 2017). The upper unit is mainly composed of thick brown-yellow massive mudstone/siltstone, which is interbedded with blue-gray thin-layered sandstone and coarse conglomerate. The conglomerate is mainly composed of metamorphic sandstone and quartzite with a southward zonal structure (**Figures 2B**,**D**, and **3E**). In the stratum, there are many mudstone layers and thin layers of gray-green massive or horizontally bedded marl containing mammalian fossils (**Figures 3C** and **D**). The lower unit contains thin grayish sandstone layers and fine-grained conglomerate but lacks a paleosol layer. The conglomerate is mainly composed of metamorphic sandstone, quartzite, and schist (Yang et al., 2017) (**Figures 2C** and **3E**).

The characteristics of the Mojiazhuang Fm. differ between two sections, as the exposure of the formation is only 20 m thick in the CJB section but more complete and thicker in the MJZ section (7–4.8 Ma, 137–0 m) (Yang et al., 2017; Zhang et al., 2017)

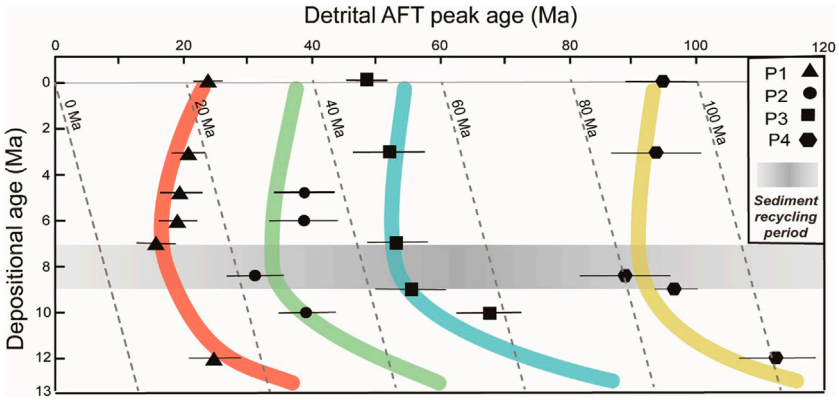

FIGURE 4 | Lag time plot of detrital AFT ages in the XB. Black symbols (P1–P4) are component ages from this study. Dashed lines are the lag time contours with corresponding lag times labeled. The peak age trend shift (peak ages progressively decrease and then increase) occurred at ~ 8 ± 1 Ma for P1, P2, P3, and P4, where each are considered to represent the time of a significant sediment recycling event.

(**Figures 2**, **3**). In the MJZ section, this formation is mainly composed of a very thick gray conglomerate with a thin layer of light brown gravelly siltstone, and the conglomerate features a massive structure, poor sorting, and miscellaneous basal support (**Figure 2A**, **3A**, and **B**). The Mojiazhuang Fm. in the CJB section mainly consists of fluvial to lacustrine red beds and contains gravel sediments from terraces (Zhang et al., 2017) (**Figure 2**). The gravel composition, paleocurrent direction, and sedimentary facies and structure in the CJB section are similar to those of the MJZ section, which is mainly composed of conglomerate, sandstone, mudstone, and siltstone (**Figures 3A–C**), lending support to the regional stratigraphic correlation. The gravel composition of the Mojiazhuang Fm. is mainly metamorphic sandstone, siltstone, quartz, and schist (Yang et al., 2017).

SAMPLING AND MEASURING

We collected nine ~3- to 6-kg sandstone samples from the modern Huangshui River and the sedimentary sections. Meanwhile, to identify the main source areas of the sections, researchers used paleocurrent orientations to constrain the provenance change in the sediments transported by flows. Previous paleocurrent measurements of the Mojiazhuang Fm. at the top of the CJB section suggest that flows were directed to the south or southwest (Zhang et al., 2017), whereas the Guanjiashan Fm. lacks paleocurrent direction indicators. In this study, the paleocurrent direction was supplementarily measured from the pebble–cobble imbrications in the conglomerates in the lower part of the CJB section (80 m). The data are plotted as rose diagrams to identify the source direction (**Figure 2C**). The external detector method was used for AFT dating in this study, and the detrital apatite age was calculated by the Zeta calibration method (Hurford and Green, 1983). This work was completed in the Rock-Mineral Preparation and Fission Track Dating Laboratory of the Geochemical Analysis and Testing Center, Northwest Institute of Eco-Environment and Resources, Chinese Academy of Sciences. The neutron flux was monitored with IRMM540R standard U glass. The Zeta calibration factor of 264.09 ± 6.88 was used in age dating (the Zeta calibration standards used were the Durango, Mt. Dromedary, and Fish Canyon Tuff standards). Spontaneous fission tracks in apatite were etched with 5% HNO_3 at 21°C for 20 s (Ketcham et al., 2009; Sobel and Seward, 2010). Induced fission tracks in the muscovite external detectors were etched with 40% HF at 20°C for 40 min. Fission tracks and track length measurements were counted on a Zeiss microscope at 1,000× magnification under a dry objective. We performed a $p(\chi^2)$ test of the AFT ages for each sample using the Radial Plotter program (Vermeesch, 2012; Sundell and Saylor, 2017). A $p(\chi^2)$ probability value of less than 5% is evidence that AFT ages represent a mixed age population (Galbraith and Laslett, 2005). Under that condition, the peak age of the apatite single-grain age component of each sample was determined by the Density Plotter program (Vermeesch, 2012).

RESULTS

Detrital AFT ages of all the samples are presented in **Tables 1** and **2**, and the apatite single-grain ages range from 198.61 to 5.4 Ma (**Table 1**) (**Supplementary Table S1** in the supporting information). All samples failed the $p(\chi^2)$ test, which means that the sample cooling ages were dispersed and derived from multiple sediment sources (**Figures 2**, **3**). To distinguish the stable satisfactory age populations of different sources, 113–-71 apatite grains from each sample were dated, and all samples were decomposed into 2–4 best fit peak ages (**Table 2**). **Figures 2**, **3** show each sample's age–density histogram and the peak age value of the mixture model of multiage components for kernel density estimation. Whether the sample was annealed post depositionally must be evaluated before interpreting the detrital AFT ages. The strata in the two sections in this study are approximately horizontal, and the thickness is much less than the annealing depth of the apatite samples (<3 km) (Bernet and Spiegel, 2004).

The AFT peak age component of each sample is older than the corresponding sedimentary age and changes vertically within the sections, which is not consistent with the annealing characteristics caused by post–depositional burial heating (Van der Beek et al., 2006). However, a few detrital AFT grain ages are always younger than or equal to their depositional ages. These younger AFT grain ages may indicate that the sediments may have experienced some degree of reheating or even total annealing. The track length distribution in detrital sample mixtures of differentiated lengths has been probably modified by annealing due to burial/reworking during the post depositional period. Most of our samples yielded tens of measured confined track lengths, and the *c*-axis–corrected mean track lengths of all samples ranged from 13.58 ± 1.62 μm (CJB-1) to 14.03 ± 1.54 μm (MJZ45) (**Table 1**). However, it is difficult to identify the degree of sample annealing before and after deposition based on these track lengths. The relative track length (>13 μm) distribution has ruled out significant annealing in both periods (Gallagher et al., 1998). The average measured Dpar range of the sample grains is 3.01–2.16 μm (**Table 1**). These parameters suggest that the AFT peak ages are not affected by the chemical composition or burial annealing of the grains (Gleadow et al., 1986; Donelick et al., 1990). Therefore, we rule out the possibility of thermal resetting of the detrital AFT ages by burial heating, and the single-grain and peak ages could represent exhumation information related to their provenance.

The paleocurrent direction results show that similar to the overlying Mojiazhuang Fm., the Guanjiashan Fm. presents a southward paleocurrent direction in the lower part of the CJB section. Based on the previous paleocurrent data, the Mojiazhuang Fm. and Guanjiashan Fm. in the MJZ section also have analogous southward flow directions (Yang et al., 2017), which indicate a northerly source, i.e., the Daban Shan (**Figures 1B**, **3**). In addition, when evaluating the sedimentary ages of the detrital AFT samples, the samples in the section need to interpolate the error in the depositional ages of each sample, which is thought to be less than 1.0 Ma based on the magnetostratigraphic data published by Zhang et al. (2017) and Yang et al. (2017). Furthermore, we set the sedimentary age of modern fluvial clastic sediments originating from the Daban Shan through the CJB section to 0 Ma. The plot of detrital AFT peak ages versus depositional age yields the following peaks (**Figure 4**): P1 (24.7–16.1 Ma), P2 (39.2–27.7 Ma), P3 (67.6–47.9 Ma), and P4 (111.7–82.8 Ma) (**Table 2**). The above peaks have an obvious trend from 24.7 ± 2.7 Ma, 39.2 ± 3.5 Ma, 67.6 ± 4.4 Ma, and 111.7 ± 7.3 Ma at the bottom of the section to 16.1 ± 1.3 Ma, 27.7 ± 3.7 Ma, 53.7 ± 5.8 Ma, and 82.8 ± 8.5 Ma at 8 ± 1 Ma. For samples with depositional ages of less than 7 Ma, a massive P1 peak appears at the top of the sections, and the P2 and P4 peak ages increase to 23 ± 1.7 Ma, 39.9 ± 4.4 Ma, and 93.5 ± 6.9 Ma at the top of the sections. By contrast, the AFT peak age at the top of the sequence tends to be more stable than those of the samples deposited before 8 ± 1 Ma. The 8.5–7 Ma fluctuation in the AFT peak age in the sections suggests that preexisting deposited sediments were recycled in the CJB and MJZ sections. In addition, the lag time is significantly shortened to 9.1 ± 1 Ma during the 8 ± 1 Ma sedimentary interval, indicating that strong tectonic deformation occurred on the northern margin of the XB during that period (**Figure 4**). The AFT peak age trends in the succession stratigraphy of the CJB and MJZ sections can provide evidence of recycled sediments on the northern margin of the XB (Malusà and Fitzgerald., 2020).

DISCUSSION

Sedimentary Provenance of the CJB and MJZ Sections

The basin sediments transported from the peripheral mountains record information on the cooling/exhumation evolution of the basement in the source area (Coutand et al., 2006). Hence, the unannealed AFT data in sediments can be interpreted by identifying the source area and by investigating the provenance of the sediment in the CJB and MJZ sections. The sediment accumulation in the XB since the Cenozoic has been influenced by multistage tectonic exhumation of the East Kunlun orogenic belt and the West Qinling and Qilian Shan orogenic belts. Previous studies have suggested that the aforementioned tectonic units acted as provenances supplying the basin with sediment during the early Cenozoic (Horton et al., 2004; Zhang et al., 2016; He et al., 2019). The source area of the basin after the Miocene shifted to the Qilian Shan (Daban Shan) or Laji Shan (Zhang et al., 2016) (**Figure 1C**). Furthermore, the MJZ and CJB sections comprise the uppermost horizontal sedimentary strata of the uppermost Cenozoic sequence in the XB. Their lithology and sedimentary structure characteristics are very similar, and the stratigraphic lithology has been divided into three sedimentary facies from bottom to top: floodplain, braided river, and alluvial fan (Yang et al., 2017; Zhang et al., 2017). Floodplain deposits dominate the bottom of both sections and consist of interbedded mudstone and siltstone with numerous paleosol complexes and occasional thin marl or thin sandstone beds. In the middle sequence of the section, the braided river intrusion with strong hydrodynamic forces increases the interbedding of sandstone and fine conglomerate layers. The upper part of both sections is dominated by coarse-grained alluvial fan sediments which were deposited under stronger hydrodynamic forces, forming thick pebble–pebble conglomerate beds with occasional sandstones and siltstones (Zhang et al., 2017). All the measured paleocurrent results are characterized by a dominant southerly current direction, and the sedimentary facies and stratigraphic lithology are similar, allowing correlation between the two sections. These findings suggest that the sediments from the Precambrian basement strata in the south are bounded by the Daban Shan in the eastern part of the Qilian Shan and were the main source area supplying the basin during the Late Miocene–Early Pliocene (Yang et al., 2017; Zhang et al., 2017). The generally large-diameter gravel clasts in the thick conglomerates of the sections attest to high-intensity fluid flow transport, from which it is speculated that the mountains to the north of the basin may have been greatly uplifted during this period (Yang et al., 2017). In addition, Zhang et al. (2016) argued

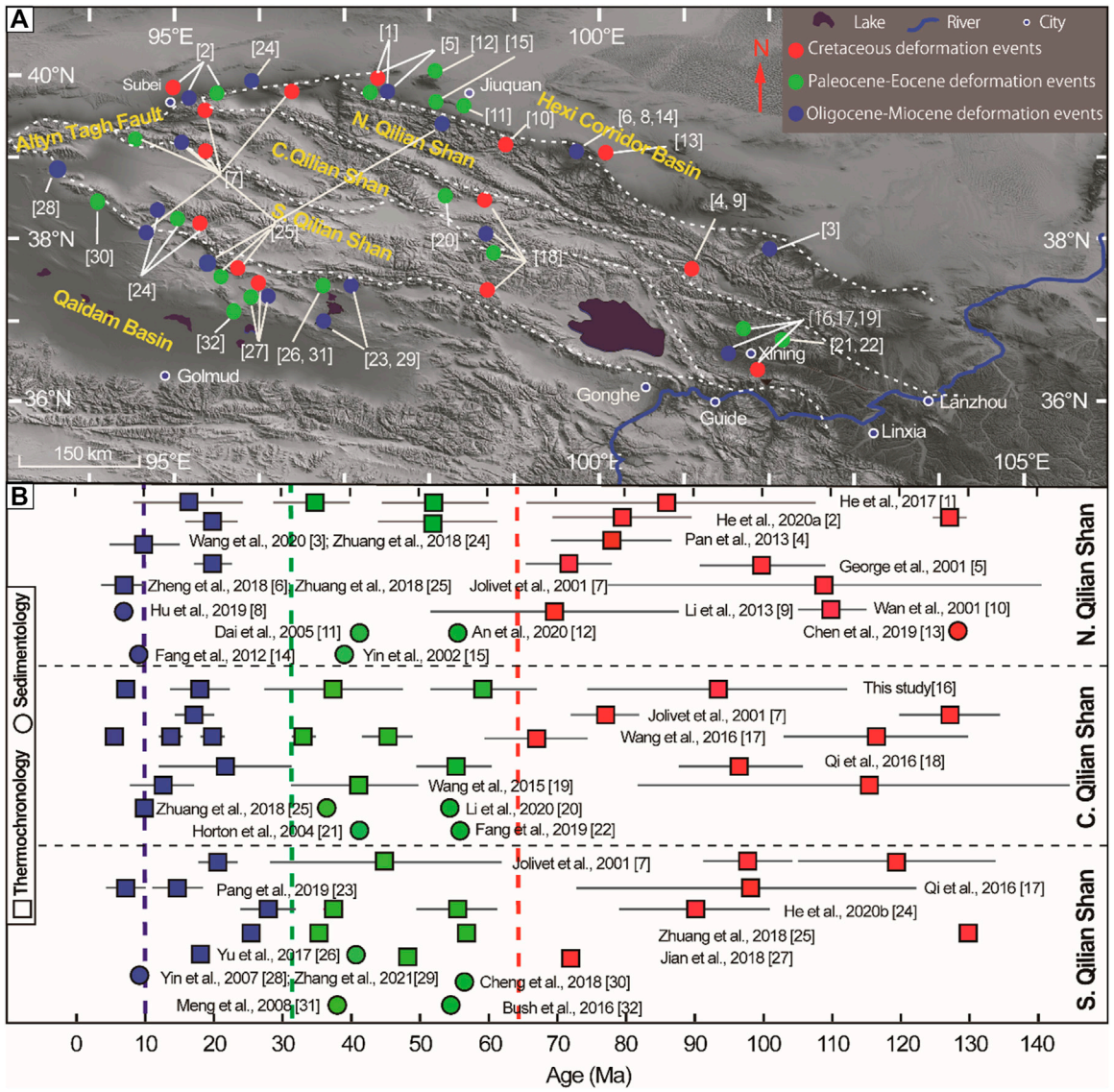

FIGURE 5 | (A) Colored dots from thermochronology and sedimentology compilation studies on the South, Central, and North Qilian Shan; the ages are denoted by points of different colors ranging from Cretaceous to Early Pliocene. The dashed white lines separate South, Central, and North Qilian Shan areas (modified from Feng and He, 1996). **(B)** Temporal distribution of the late Mesozoic–Cenozoic tectonic events recorded in the Qilian Shan, as constrained by thermochronology (squares) and sedimentology (diamonds).

that the detrital zircon ages and depositional environment changes present in the Shuiwan section indicate that rapid uplift of the Qilian Shan occurred after ca. 20 Ma. However, Lease et al. (2011, 2012) used detrital zircon ages and low-thermochronology methods to constrain the start of the accelerated growth of the WNW-trending eastern Laji Shan to ca. 24–22 Ma and north-directed Jishi Shan to ca. 13 Ma. This kinematic shift near our study area corresponds to changes in sedimentary facies present only in the Xunhua basin (located to the south of the Laji Shan), while the sedimentary environment and provenance changes in the XB experienced no significant shift during the corresponding time. Recently, Nd and Pb isotope analyses of the Cenozoic strata in the XB have provided robust evidence showing that the proportion of sediment input from the Qilian Shan increased and represented ~70–35% after the Early Miocene (He et al., 2019). In summary, the unannealed AFT ages of the sediments in the CJB and MJZ sections effectively document the exhumation and deformation of the Qilian Shan.

Pre-Cenozoic Exhumation Events

The new AFT data present multistage Mesozoic–Cenozoic tectonic dynamic evolution events based on material sourced from the Qilian Shan. The oldest Late Cretaceous signal P4 (111.7–82.8 Ma), which was also identified in the AFT analysis by Wang et al. (2016), formed prior to the Late Miocene sediment sequence in the XB. Similar bedrock thermal simulation AFT age

signals are widely exposed in the northern XB and northwestern Qilian Shan (George et al., 2001; Jolivet et al., 2001; Pan et al., 2013; Wang et al., 2015a; Qi et al., 2016; Wang et al., 2020). In addition, the XB, Qaidam Basin, and Hexi Corridor Basin have received Qilian Shan sediments, and the abundant clastic material with Late Cretaceous cooling ages and the widespread angular and parallel unconformities between the Cenozoic and Late Cretaceous strata indicate that a significant tectonic event occurred during the Late Cretaceous to Early Cenozoic (Bureau of Geological and Mineral Resources of Qinghai Province (BGMRQP); Gansu Geological Bureau, 1989; Abels et al., 2001; Pullen et al., 2008; Wan et al., 2010; Li et al., 2013; Ding et al., 2017; Zuza et al., 2018; Chen et al., 2019; Lin et al., 2019; Pang et al., 2019b; He et al., 2020a; He et al., 2020b) (**Figure 5**). These characteristics in the Qilian Shan have also been observed elsewhere in northern Tibet, and low-temperature thermochronological evidence indicates that Late Cretaceous to early Eocene exhumation events were widespread regional events (Jian et al., 2018). Thermochronological evidence and paleoelevation estimates also suggest rapid to moderate cooling and substantial surface elevation gain in central Tibet during the Cretaceous to Eocene (Kapp et al., 2003; Wang et al., 2008; Rowley and Currie, 2006; Ding et al., 2017). This situation implies that the Andean-type northward subduction of the Neo-Tethys oceanic plate during the Cretaceous led to thickening of the north Tibet lithosphere (Staisch et al., 2016; Allen et al., 2017; Ding et al., 2017; Lippert et al., 2014). These events may have been caused by the closure of the Mesozoic Tethys in the southern Qaidam Basin, which acted as the force driving Cretaceous tectonic activity on the northern plateau (Vincent & Allen, 1999; Yin and Harrison, 2000; Jolivet et al., 2001; Pullen et al., 2008; Duvall et al., 2013; Jian et al., 2018). The north-directed Lhasa–Asian Plate collision triggered northeastward sinistral strike-slip activity on the Altyn and Kunlun faults in the Jurassic–Late Cretaceous (Murphy et al., 1997; Liu et al., 2000; Ritts and Biffi, 2000; Yin and Harrison, 2000; Jolivet et al., 2001; Sobel et al., 2001; Kapp et al., 2005; Liu et al., 2005; Tian et al., 2014; Kapp et al., 2015). Although the amount of crustal thickening and pervasive suture zones in the northeastern Tibetan Plateau prior to the collision remain unclear, the new detrital AFT analysis results in this study indicate that the widespread pre-collisional deformation region may have influenced the tectonics of the current northern margin of the Tibetan Plateau.

Cenozoic Multistage Tectonism Exhumation Events

Evidence of Cenozoic deformation in the Qilian Shan is concentrated in the suture zone of the ancient block, and this zone has inherited the tectonic activity properties of the pre-Cenozoic structures (Zuza et al., 2016, 2018). Based on dated unannealed detrital AFT ages and previous thermochronological and sedimentological studies, we infer that the CJB and MJZ sections record three exhumation stages representing the Qilian Shan tectonic evolution during the Cenozoic. The detrital AFT peak age P3 (67.7–47.9 Ma) reveals that the first stage of Paleocene–Early Eocene tectonic reactivation in the Qilian Shan occurred almost synchronously with the initial India–Asia collision (An et al., 2020; He et al., 2020a). At this time, the detrital accumulation rate accelerated in the Qijiachuan Fm. (54–51.8 Ma), and the XB experienced clockwise vertical axis block rotation (Horton et al., 2004), both of which reflect the growth of the Qilian Shan during the early Cenozoic (Fang et al., 2019). Similar scenarios are observed in the Qilian Shan and northern Qaidam basins, in which contemporaneous tectonic exhumation events were associated with exhumation, the onset of coarse sediment deposition, sedimentation rate acceleration, and unconformity development (Horton et al., 2004; Yin et al., 2002; Meng and Fang, 2008; Yin et al., 2008; Bush et al., 2016; Qi et al., 2016; He et al., 2017; Jian et al., 2018; Zhuang et al., 2018; Cheng et al., 2019; An et al., 2020; He et al., 2020a; He et al., 2020b; Cheng et al., 2021) (**Figure 5**), but none received large quantities of clasts from the Qilian Shan deposited on the Hexi Corridor during the corresponding time (Dai et al., 2005; Bovet et al., 2009). Accompanying the initial Indian–Asian Plate collision, the early Cenozoic deformation was also roughly stratigraphically consistent with cooling events in the northeastern part of the plateau, such as the Jiuquan basin (He et al., 2018; Lin et al., 2019), Lanzhou basin (Yue et al., 2000; Fang et al., 2007), East Kunlun Shan (Duvall et al., 2011; Duvall et al., 2013), Altyn fault (Mock et al., 1999; Jolivet et al., 2001), Haiyuan-Liupan Shan (Lin et al., 2011), and West Qinling (Clark et al., 2010).

The second-stage age populations with peaks at P2 (39.2–27.7 Ma) and P1 (24.7–16.1 Ma) indicate that the Qilian Shan was subjected to a series of exhumation events that occurred in the Late Eocene–Oligocene and Early Miocene. Thermochronological studies identifying Eocene–Early Miocene tectonic events have also been based on detrital and *in situ* AFT age signals in the Qaidam Basin, Hexi Corridor Basin, Qilian Basin, and Qilian Shan (Jolivet et al., 2001; Zheng et al., 2010; Qi et al., 2016; He et al., 2017; Zhang et al., 2018; Zhuang et al., 2018; Yu et al., 2019; An et al., 2020; He et al., 2020a; He et al., 2020b) (**Figure 5**). In addition, sedimentological studies have emphasized that in the Eocene–Oligocene, thrusting continued to progress in the Qilian Shan (Yin et al., 2002; Yin et al., 2008; Cheng et al., 2019). As a result, the sedimentary environment changed from a dry salt lake to a floodplain from the Mahalagou Fm. to the Xiejia Fm., and a growth strata relationship formed between the two groups at the edge of the XB (Fang et al., 2019). An analysis of the Early Miocene provenance also suggests that the primary provenance of the XB was the Qilian orogenic belt, while the Laji Shan represented a secondary provenance, indicating that the Qilian Shan experienced tectonic exhumation during this episode (Lease et al., 2011; Xiao et al., 2012; Wang et al., 2016; Zhang et al., 2016; Wang et al., 2017). The corresponding episodes of bedrock exhumation in the Qilian Shan are also confirmed by the marked increase in the accumulation rate and sediment flux in the Qaidam Basin and Hexi Corridor Basin (Jian et al., 2013; Wang et al., 2017; Jian et al., 2018; Zhuang et al., 2018; Zhuang et al., 2019) (**Figure 5**). The oldest Cenozoic sediments in the Hexi Corridor is the Huoshaogou Fm., where the sequence presence of the thick alluvial fan conglomeration at the bottom of the foreland basin may indicate the initial deformation and uplift of the northern

Qilian Shan (Dai et al., 2005; Bovet et al., 2009; Guo et al., 2009). This process is driven by the Altyn faults and Kunlun fault that thrust onto the Hexi Corridor Basin, Muli Basin, and Qaidam Basin from its foreland margins (Cheng et al., 2018; Qi et al., 2013; Qi et al., 2015; Yu et al., 2017; Zhuang et al., 2018; Zhuang et al., 2019). The Altyn fault and East Kunlun Shan exhumation events also indicate that the crust of the northeastern margin of the Tibetan Plateau continued to thicken and grow outward after plate collision (Mock et al., 1999; Ritts et al., 2004; Molnar and Stock, 2009; Clark et al., 2010; Zhuang et al., 2011).

During the last stage, the reversal of the AFT peak ages at 8 ± 1 Ma in the CJB and MJZ sections suggests that the late Miocene sediment recycling in the XB may have been caused by tectonic deformation (**Figure 4**). The detritus was eroded from the sequence before the Mojiazhuang Fm. was deposited starting at ca.8 Ma, and it was temporarily stored in the XB, where it was not affected by post depositional annealing (peak age components include P2, P3, and P4). Starting from 8.5 Ma (MJZ195), thrust fault activity controlled the uplift and erosion of sediment previously stored in the XB wedge-top basin. Thus, sediment reworked from pre-8 Ma samples was transported to the final sink and mixed with sediment derived from erosion after 8 Ma, forming a new sedimentary unit. This scenario suggests that long-term sediment storage and reworking have affected the thermochronological age trends. Detritus derived from erosion of pre-8 Ma sediment, and temporarily stored in a wedge-top basin (for example) after 8 Ma was reworked and mixed into the final sink along with detritus derived from the erosion of previously stored material. As a result, the samples with sediment recycling (MJZ95, MJZ45, MJZ15, CJB-1, and modern river samples) are expected to include not only the peak (P1) defined by the AFT ages measured in mineral grains but also all the major grain-age populations inherited from the Guanjiashan Fm. Only the smallest grain-age populations of the Guanjiashan Fm. are prone to remain undetected in the Mojiazhuang Fm. because they may fall below the detection limit after sediment mixing (Vermeesch, 2012). In the Mojiazhuang Fm., the age peaks inherited from recycled sediments are invariably older than the age peaks derived from erosion of the Guanjiashan Fm. The Mojiazhuang Fm. includes all the major AFT age populations detected in the underlying late Miocene–Pliocene formations of the CJB and MJZ succession, which is consistent with recycling of specific intervals of a stratigraphic succession within a basin after long-term storage and reworking (Malusà and Fitzgerald, 2020). Thermal modeling of the AFT data and analysis of the heavy minerals in the Laji Shan bedrock also suggest that the exhumation stage occurred in the Late Miocene (8–4 Ma) (Wang et al., 2016). In addition, the rapid increase in the gravel diameter and coarse conglomerate content from the Guanjiashan Fm. to the Mojiazhuang Fm. reflects a sharp rise in the sedimentation rate during this period (Yang et al., 2017; Fang et al., 2019). Evidence of growth strata and climate proxies in the Jiuquan Basin and Qaidam Basin also reflects the strike-slip thrust system activity in the Qilian Shan building high topography from the Late Miocene to the Pliocene (Bao et al., 2019;Yin et al., 2008; Zheng et al., 2010; Wang et al., 2017; Zheng et al., 2017; Zhang et al., 2018; Zhuang et al., 2018; Chen et al., 2019; Fang et al., 2019; Hu et al., 2019; Pang et al., 2019a, Zhang et al., 2021) (**Figure 5**). Several previous studies also underlined the Miocene acceleration motions of the major strike-slip faults adjacent to the basin, which are significant for exploring the proximal exhumation. Current evidence suggests that the left-slip Haiyuan fault initiated at ca. 16 Ma (e.g., Li et al., 2019, 2020; Duvall et al., 2013; Zhang et al., 2020), but the right-slip Riyueshan and Elashan faults may also be slightly younger, i.e., closer to ca. 10 Ma (Yuan et al., 2011; Cheng et al., 2021). In addition, Lease et al. (2011) through apatite (U-Th)/He dating analysis revealed that the accelerated growth of the WNW-trending eastern Laji Shan began at ca. 24–22 Ma and that growth of the north-trending Jishi Shan did not commence until ca. 13 Ma. Noticeably, the tectonic activity in the Late Miocene is also confirmed by the increase in the large number of Miocene deformation tectonothermal events that occurred on the northeastern margin of the Tibetan Plateau (ca. 15–5 Ma), as evidenced by AFT and (U-Th)/He data similar to our data, and the reorganization of deformation along the Qilian Shan fault (Lease et al., 2011; Yuan et al., 2011; Craddock et al., 2012; Duvall et al., 2012; Lease et al., 2012; Yuan et al., 2013) and the West Qinling and Eastern Kunlun faults (Clark et al., 2010; Lin et al., 2011; Duvall et al., 2013; Wang et al., 2020). Collectively, the scattered Early Miocene deformation in the major left-lateral strike-slip faults was followed by widespread late Miocene deformation associated with right-lateral slip in the Qilian Shan (**Figure 5**). Therefore, we speculate that the deformation situation related to the kinematic shift in northeastern Tibet is compatible with west–east crustal stretching/lateral displacement, nonrigid off-fault deformation, and broad clockwise rotation and bookshelf faulting, which together accommodate northeast–southwest India–Asia convergence (Cheng et al., 2021).

In summary, the comprehensive analysis of the Qilian Shan AFT data revealed that the mountain range experienced initial tectonic exhumation events in the early Cenozoic in quasi-synchronous response to the Indian–Asian Plate collision, as supported by the previous results of sedimentological studies. During the Oligocene–Miocene period, the combined action of multistage deformation caused the plateau to thicken and expand outward after plate collision. Thus, during this period, the influence of this plate collision propagated nearly instantaneously to different regions in the northeastern Tibetan Plateau. In the Late Miocene, the uplift of the Qilian Shan caused a sediment recycling event. Our findings indicate that the Tibetan Plateau gained elevation in the Mesozoic–Early Cenozoic, driven by the convergence of different blocks. This plateau growth scenario seems to be incompatible with the deforming viscous mantle lithosphere model (Clark, 2012; Clark et al., 2010; Yin et al., 2008), which predicts that the entire plateau has shortened at a constant strain rate over time. An important caveat of the applicability of this model is the pervasive suture zones in the Qilian Shan and even the Eastern Kunlun range (Allen et al., 2017). Without these weak zones, the NE Tibetan Plateau deformation may not have so easily reactivated and resulted in quasi-synchronous deformation in

the early stage of the collision, which was accompanied by region-specific amplitudes (Zuza et al., 2016; Jian et al., 2018; Zuza et al., 2018; Cheng et al., 2021). The late Miocene deformation of the plateau seriously influenced the climatic and paleogeographic pattern evolution (Li et al., 2021; Zhang et al., 2017).

CONCLUSION

Through AFT analysis of Late Miocene to Early Pliocene synorogenic sediments in the XB, we discussed the exhumation history of the Qilian Shan. Based on the AFT dating results from these sediments, the earliest exhumation phase occurred during the Late Cretaceous. The results reveal both the pre-Cenozoic growth history and the Cenozoic deformation mechanism of the Qilian Shan and other regions along the northeastern margin of the Tibetan Plateau. The early Cenozoic detrital AFT age group suggests that the block (as the source of the studied sediments) responded quasi-synchronously to the initial Indian–Asian Plate collision. The present geomorphology in the Qilian Shan has experienced multistage tectonic exhumation overprinting from the late Mesozoic to the late Cenozoic. The results from this study, as well as related findings from other regions of the northeastern Tibetan Plateau, provide new insights into the paleogeographic pattern evolution.

DATA AVAILABILITY STATEMENT

The original contributions presented in the study are included in the article/**Supplementary Material**, and further inquiries can be directed to the corresponding author.

AUTHOR CONTRIBUTIONS

LC contributed in writing, reviewing, and editing, data curation, writing—original draft preparation; CS and XF contributed in supervision, project administration, and funding acquisition; YW contributed to writing—original draft; PH contributed to formal analysis, validation, and methodology; YZ, JZ, and YC contributed to visualization and investigation.

FUNDING

This work was co-supported by the Second Tibetan Plateau Scientific Expedition (STEP) program (Grant No. 2019QZKK0707), the Strategic Priority Research Program of Chinese Academy of Sciences (Grant No. XDA200702012) and the National Natural Science Foundation of China (Grant No. 41902223 and 41872098).

ACKNOWLEDGMENTS

We express our cordial thanks to Tao Zhang for the valuable comments that improved the manuscript. We also thank Lijie Yao, Pengfei Chang, and Bo Ren for their assistance in the field and laboratory.

SUPPLEMENTARY MATERIAL

The Supplementary Material for this article can be found online at: https://www.frontiersin.org/articles/10.3389/feart.2021.760100/full#supplementary-material

REFERENCES

Abels, H. A., Dupont-Nivet, G., Xiao, G., Bosboom, R., and Krijgsman, W. (2011). Step-wise Change of Asian interior Climate Preceding the Eocene-Oligocene Transition (EOT). *Palaeogeogr. Palaeoclimatol. Palaeoecol.* 299, 399–412. doi:10.1016/j.palaeo.2010.11.028

Allen, M. B., Walters, R. J., Song, S., Saville, C., De Paola, N., Ford, J., et al. (2017). Partitioning of Oblique Convergence Coupled to the Fault Locking Behavior of Fold-And-Thrust Belts: Evidence from the Qilian Shan, Northeastern Tibetan Plateau. *Tectonics* 36 (12), 1679–1698. doi:10.1002/2017tc004476

An, K., Lin, X., Wu, L., Yang, R., Chen, H., Cheng, X., et al. (2020). An Immediate Response to the Indian-Eurasian Collision along the Northeastern Tibetan Plateau: Evidence from Apatite Fission Track Analysis in the Kuantan Shan-Hei Shan. *Tectonophysics* 774, 228278. doi:10.1016/j.tecto.2019.228278

Bao, J., Song, C., Yang, Y., Fang, X., Meng, Q., Feng, Y., et al. (2019). Reduced Chemical Weathering Intensity in the Qaidam Basin (NE Tibetan Plateau) during the Late Cenozoic. *J. Asian Earth Sci.* 170, 155–165. doi:10.1016/j.jseaes.2018.10.018

Baotian, P., Qingyang, L., Xiaofei, H., Haopeng, G., Zibian, L., Shaofei, J., et al. (2013). Cretaceous and Cenozoic Cooling History of the Eastern Qilian Shan, north-eastern Margin of the Tibetan Plateau: Evidence from Apatite Fission-Track Analysis. *Terra Nova* 25 (6), 431–438. doi:10.1111/ter.12052

Bernet, M., and Spiegel, C. (2004). Introduction: Detrital Thermochronology. *Detrital Thermochronology*, 1–6. doi:10.1130/0-8137-2378-7.1

Bovet, P. M., Ritts, B. D., Gehrels, G., Abbink, A. O., Darby, B., and Hourigan, J. (2009). Evidence of Miocene Crustal Shortening in the North Qilian Shan from Cenozoic Stratigraphy of the Western Hexi Corridor, Gansu Province, China. *Am. J. Sci.* 309 (4), 290–329. doi:10.2475/00.4009.02

Bureau of Geological and Mineral Resources of Qinghai Province (BGMRQP) (1985). *Regional Geological Survey Reports of Duoba, Xining, Tianjiazhai and Gaodian Sheets (1: 50000), Qinghai Province, PR China*.

Bush, M. A., Saylor, J. E., Horton, B. K., and Nie, J. (2016). Growth of the Qaidam Basin during Cenozoic Exhumation in the Northern Tibetan Plateau: Inferences from Depositional Patterns and Multiproxy Detrital Provenance Signatures. *Lithosphere* 8, 58–82. doi:10.1130/l449.1

Chen, X. H., Shao, Z., Xiong, X., Gao, R., Xu, S., Zhang, Y., et al. (2019). Early Cretaceous Overthrusting of Yumu Mountain and Hydrocarbon prospect on the Northern Margin of the Qilian Orogenic belt. *Acta Geoscientica Sinica* 40 (3), 377–392. doi:10.3975/cagsb.2019.050901

Chen, Y., Gilder, S., Halim, N., Cogné, J. P., and Courtillot, V. (2002). New Paleomagnetic Constraints on central Asian Kinematics: Displacement along the Altyn Tagh Fault and Rotation of the Qaidam Basin. *Tectonics* 21 (5), 1042. doi:10.1029/2001tc901030

Cheng, F., Garzione, C. N., Garzione, C. N., Mitra, G., Guo, Z., Lu, H., et al. (2018). The Interplay between Climate and Tectonics during the Upward and Outward Growth of the Qilian Shan Orogenic Wedge, Northern Tibetan Plateau. *Earth-Science Rev.* 287, 3. doi:10.1130/abs/2018AM-316434

Cheng, F., Garzione, C. N., Mitra, G., Jolivet, M., Guo, Z., Lu, H., et al. (2019). The Interplay between Climate and Tectonics during the Upward and Outward

Growth of the Qilian Shan Orogenic Wedge, Northern Tibetan Plateau. *Earth-Science Rev.* 198, 102945. doi:10.1016/j.earscirev.2019.102945

Cheng, F., Zuza, A. V., Haproff, P. J., Wu, C., Neudorf, C., Chang, H., et al. (2021). Accommodation of India-Asia Convergence via Strike-Slip Faulting and Block Rotation in the Qilian Shan Fold-Thrust belt, Northern Margin of the Tibetan Plateau. *J. Geol. Soc.* 178 (3), jgs2020–207. doi:10.1144/jgs2020-207

Clark, M. K. (2012). Continental Collision Slowing Due to Viscous Mantle Lithosphere rather Than Topography. *Nature* 483 (7387), 74–77. doi:10.1038/nature10848

Clark, M. K., Farley, K. A., Zheng, D., Wang, Z., and Duvall, A. R. (2010). Early Cenozoic Faulting of the Northern Tibetan Plateau Margin from Apatite (U-Th)/He Ages. *Earth Planet. Sci. Lett.* 296 (1-2), 78–88. doi:10.1016/j.epsl.2010.04.051

Coutand, I., Carrapa, B., Deeken, A., Schmitt, A. K., Sobel, E. R., and Strecker, M. R. (2006). Propagation of Orographic Barriers along an Active Range Front: Insights from sandstone Petrography and Detrital Apatite Fission-Track Thermochronology in the Intramontane Angastaco basin, NW Argentina. *Basin Res.* 18 (1), 1–26. doi:10.1111/j.1365-2117.2006.00283.x

Craddock, W. H., Kirby, E., Dewen, Z., and Jianhui, L. (2012). Tectonic Setting of Cretaceous Basins on the NE Tibetan Plateau: Insights from the Jungong basin. *Basin Res.* 24, 51–69. doi:10.1111/j.1365-2117.2011.00515.x

Dai, S., Fang, X., Song, C., Gao, J., Gao, D., and Li, J. (2005). Early Tectonic Uplift of the Northern Tibetan Plateau. *Chin. Sci Bull* 50, 1642–1652. doi:10.1360/03wd0255

Dayem, K. E., Molnar, P., Clark, M. K., and Houseman, G. A. (2009). Far-field Lithospheric Deformation in Tibet during continental Collision. *Tectonics* 28, a–n. doi:10.1029/2008TC002344

Ding, L., Spicer, R. A., Yang, J., Xu, Q., Cai, F., Li, S., et al. (2017). Quantifying the Rise of the Himalaya Orogen and Implications for the South Asian Monsoon. *Geology* 45, 215–218. doi:10.1130/g38583.1

Donelick, R. A., Roden, M. K., Mooers, J. D., Carpenter, B. S., and Miller, D. S. (1990). Etchable Length Reduction of Induced Fission Tracks in Apatite at Room Temperature (≈ 23°C): Crystallographic Orientation Effects and "initial" Mean Lengths. *Int. J. Radiat. Appl. Instrumentation. D. Nucl. Tracks Radiat. Measurements* 17 (3), 261–265. doi:10.1016/1359-0189(90)90044-x

Dupont-Nivet, G., Hoorn, C., and Konert, M. (2008). Erratum. *Geology* 37 (6), 506. doi:10.1130/0091-7613-37.6.506

Dupont-Nivet, G., Horton, B. K., Butler, R. F., Wang, J., Zhou, J., and Waanders, G. L. (2004). Paleogene Clockwise Tectonic Rotation of the Xining-Lanzhou Region, Northeastern Tibetan Plateau. *J. Geophys. Res.* 109 , B04401. doi:10.1029/2003JB002620

Duvall, A. R., Clark, M. K., Avdeev, B., Farley, K. A., and Chen, Z. (2012). Widespread Late Cenozoic Increase in Erosion Rates across the interior of Eastern Tibet Constrained by Detrital Low-Temperature Thermochronometry. *Tectonics* 31 (3), a–n. doi:10.1029/2011tc002969

Duvall, A. R., Clark, M. K., Kirby, E., Farley, K. A., Craddock, W. H., Li, C., et al. (2013). Low-temperature Thermochronometry along the Kunlun and Haiyuan Faults, NE Tibetan Plateau: Evidence for Kinematic Change during Late-Stage Orogenesis. *Tectonics* 32 (5), 1190–1211. doi:10.1002/tect.20072

Duvall, A. R., Clark, M. K., Van der Pluijm, B. A., and Li, C. (2011). Direct Dating of Eocene Reverse Faulting in Northeastern Tibet Using Ar-Dating of Fault Clays and Low-Temperature Thermochronometry. *Earth Planet. Sci. Lett.* 304, 520–526. doi:10.1016/j.epsl.2011.02.028

England, P., and Houseman, G. (1986). Finite Strain Calculations of continental Deformation: 2. Comparison with the India-Asia Collision Zone. *J. Geophys. Res.* 91 (B3), 3664–3676. doi:10.1029/jb091ib03p03664

Fang, X., Liu, D., Song, C., Dai, S., and Meng, Q. (2012). Oligocene Slow and Miocene-Quaternary Rapid Deformation and Uplift of the Yumu Shan and north Qilian Shan: Evidence from High-Resolution Magnetostratigraphy and Tectonosedimentology. *Geol. Soc. Lond. Spec. Publications* 373 (1), 149–171. doi:10.1144/sp373.5

Fang, X., Zhang, W., Meng, Q., Gao, J., Wang, X., King, J., et al. (2007). High-resolution Magnetostratigraphy of the Neogene Huaitoutala Section in the Eastern Qaidam Basin on the NE Tibetan Plateau, Qinghai Province, China and its Implication on Tectonic Uplift of the NE Tibetan Plateau. *Earth Planet. Sci. Lett.* 258 (1-2), 293–306. doi:10.1016/j.epsl.2007.03.042

Fang, X., Zhao, Z., Li, J., Yan, M., Pan, B., Song, C., et al. (2005). Magnetostratigraphy of the Late Cenozoic Laojunmiao Anticline in the Northern Qilian Mountains and its Implications for the Northern Tibetan Plateau Uplift. *Sci. China Ser. D* 48 (7), 1040–1051. doi:10.5483/BMBRep.2008.41.5.353

Fang, X., Fang, Y., Zan, J., Zhang, W., Song, C., Appel, E., et al. (2019). Cenozoic Magnetostratigraphy of the Xining Basin, NE Tibetan Plateau, and its Constraints on Paleontological, Sedimentological and Tectonomorphological Evolution. *Earth-Science Rev.* 190, 460–485. doi:10.1016/j.earscirev.2019.01.021

Feng, Y., and He, S. (1996). *Tectonics and Orogeny in Qilian Mountains (In Chinese)*. Beijing: Geological Publishing House.

Galbraith, R. F., and Laslett, G. M. (1993). Statistical Models for Mixed Fission Track Ages. *Nucl. tracks Radiat. measurements* 21 (4), 459–470. doi:10.1016/1359-0189(93)90185-C

Gallagher, K., Brown, R., and Johnson, C. (1998). Fission Track Analysis and its Applications to Geological Problems. *Annu. Rev. Earth Planet. Sci.* 26 (1), 519–572. doi:10.1146/annurev.earth.26.1.519

Gehrels, G. E., Yin, A., and Wang, X.-F. (2003). Magmatic History of the Northeastern Tibetan Plateau. *J. Geophys. Res.* 108 (B9), 2423. doi:10.1029/2002JB001876

Gansu Geologic Bureau (1989). *Regional Geology Evolution of Gansu Province [in Chinese]*. Beijing: Geological Publishing House.

George, A. D., Marshallsea, S. J., Wyrwoll, K.-H., Jie, C., and Yanchou, L. (2001). Miocene Cooling in the Northern Qilian Shan, Northeastern Margin of the Tibetan Plateau, Revealed by Apatite Fission-Track and Vitrinite-Reflectance Analysis. *Geol* 29, 9392–9942.

Gleadow, A. J. W., Duddy, I. R., Green, P. F., and Hegarty, K. A. (1986). Fission Track Lengths in the Apatite Annealing Zone and the Interpretation of Mixed Ages. *Earth Planet. Sci. Lett.* 78 (2-3), 245–254. doi:10.1016/0012-821x(86)90065-8

Guo, Z., Lu, J., and Zhang, Z. (2009). Cenozoic Exhumation and Thrusting in the Northern Qilian Shan, Northeastern Margin of the Tibetan Plateau: Constraints from Sedimentological and Apatite Fission-Track Data. *Acta Geologica Sinica (English edition)* 83, 562–579. doi:10.1111/j.1755-6724.2009.00045.x

Harrison, T. M., Copeland, P., Kidd, W. S. F., and Yin, A. (1992). Raising Tibet. *Science* 255 (5052), 1663–1670. doi:10.1126/science.255.5052.1663

He, P., Song, C., Wang, Y., Chen, L., Chang, P., Wang, Q., et al. (2017). Cenozoic Exhumation in the Qilian Shan, Northeastern Tibetan Plateau: Evidence from Detrital Fission Track Thermochronology in the Jiuquan Basin. *J. Geophys. Res. Solid Earth* 122 (8), 6910–6927. doi:10.1002/2017JB014216

He, P., Song, C., Wang, Y., Meng, Q., Chen, L., Yao, L., et al. (2018). Cenozoic Deformation History of the Qilian Shan (Northeastern Tibetan Plateau) Constrained by Detrital Apatite Fission-Track Thermochronology in the Northeastern Qaidam Basin. *Tectonophysics* 749, 1–11. doi:10.1016/j.tecto.2018.10.017

He, P., Song, C., Wang, Y., Meng, Q., Wang, D., Feng, Y., et al. (2020a). Early Cenozoic Exhumation in the Qilian Shan, Northeastern Margin of the Tibetan Plateau: Insights from Detrital Apatite Fission Track Thermochronology. *Terra Nova* 32, 415–424. doi:10.1111/ter.12478

He, P., Song, C., Wang, Y., Wang, D., Chen, L., Meng, Q., et al. (2021b). Early Cenozoic Activated Deformation in the Qilian Shan, Northeastern Tibetan Plateau: Insights from Detrital Apatite Fission-track Analysis. *Basin Res.* 33, 1731–1748. doi:10.1111/bre.12533

He, Z., Guo, Z., Yang, F., Sayem, A. S. M., Wu, H., Zhang, C., et al. (2019). Provenance of Cenozoic Sediments in the Xining Basin Revealed by Nd and Pb Isotopic Evidence: Implications for Tectonic Uplift of the NE Tibetan Plateau. *Geochem. Geophys. Geosystems* 20, 4531–4544. doi:10.1029/2019gc008556

Hong, D., Jian, X., Fu, L., and Zhang, W. (2020). Garnet Trace Element Geochemistry as a Sediment Provenance Indicator: An Example from the Qaidam basin, Northern Tibet. *Mar. Pet. Geology.* 116, 104316. doi:10.1016/j.marpetgeo.2020.104316

Horton, B. K., Dupont-Nivet, G., Zhou, J., Waanders, G. L., Butler, R. F., and Wang, J. (2004). Mesozoic-Cenozoic Evolution of the Xining-Minhe and Dangchang Basins, Northeastern Tibetan Plateau: Magnetostratigraphic and Biostratigraphic Results. *J. Geophys. Res.* 109 (B4). doi:10.1029/2003JB002913

Hu, X., Chen, D., Pan, B., Chen, J., and Zhao, Q. (2019). Sedimentary Evolution of the Foreland basin in the NE Tibetan Plateau and the Growth of the Qilian Shan since 7Ma. *Geol. Soc. America Bull.* 131, 1744–1760. doi:10.1130/B35106.1

Hurford, A. J., and Green, P. F. (1983). The Zeta Age Calibration of Fission-Track Dating. *Chem. Geology.* 41, 285–317. doi:10.1016/s0009-2541(83)80026-6

Jian, X., Guan, P., Zhang, D.-W., Zhang, W., Feng, F., Liu, R.-J., et al. (2013). Provenance of Tertiary sandstone in the Northern Qaidam basin, Northeastern Tibetan Plateau: Integration of Framework Petrography, Heavy mineral Analysis and mineral Chemistry. *Sediment. Geology.* 290, 109–125. doi:10.1016/j.sedgeo.2013.03.010

Jian, X., Guan, P., Zhang, W., Liang, H., Feng, F., and Fu, L. (2018). Late Cretaceous to Early Eocene Deformation in the Northern Tibetan Plateau: Detrital Apatite Fission Track Evidence from Northern Qaidam basin. *Gondwana Res.* 60, 94–104. doi:10.1016/j.gr.2018.04.007

Jolivet, M., Brunel, M., Seward, D., Xu, Z., Yang, J., Roger, F., et al. (2001). Mesozoic and Cenozoic Tectonics of the Northern Edge of the Tibetan Plateau: Fission-Track Constraints. *Tectonophysics* 343 (1-2), 111–134. doi:10.1016/S0040-1951(01)00196-2

Kapp, P., Taylor, M., Stockli, D., and Ding, L. (2008). Development of Active Low-Angle normal Fault Systems during Orogenic Collapse: Insight from Tibet. *Geol* 36 (1), 7–10. doi:10.1130/G24054A.1

Kapp, P., Yin, A., Harrison, T. M., and Ding, L. (2005). Cretaceous-Tertiary Shortening, basin Development, and Volcanism in central Tibet. *Geol. Soc. America Bull.* 117 (7–8), 865–878. doi:10.1130/B25595.1

Kapp, P., Yin, A., Manning, C. E., Harrison, T. M., Taylor, M. H., and Ding, L. (2003). Tectonic Evolution of the Early Mesozoic Blueschist-Bearing Qiangtang Metamorphic belt, central Tibet. *Tectonics* 22, a–n. doi:10.1029/2002tc001383

Ketcham, R. A., Donelick, R. A., Balestrieri, M. L., and Zattin, M. (2009). Reproducibility of Apatite Fission-Track Length Data and thermal History Reconstruction. *Earth Planet. Sci. Lett.* 284 (3-4), 504–515. doi:10.1016/j.epsl.2009.05.015

Lease, R. O., Burbank, D. W., Clark, M. K., Farley, K. A., Zheng, D., and Zhang, H. (2011). Middle Miocene Reorganization of Deformation along the Northeastern Tibetan Plateau. *Geology* 39 (4), 359–362. doi:10.1130/g31356.1

Lease, R. O., Burbank, D. W., Hough, B., Wang, Z., and Yuan, D. (2012). Pulsed Miocene Range Growth in Northeastern Tibet: Insights from Xunhua Basin Magnetostratigraphy and Provenance. *Geol. Soc. America Bull.* 124 (5–6), 657–677. doi:10.1130/B30524.1

Li, B., Chen, X., Zuza, A. V., Hu, D., Ding, W., Huang, P., et al. (2019). Cenozoic Cooling History of the North Qilian Shan, Northern Tibetan Plateau, and the Initiation of the Haiyuan Fault: Constraints from Apatite- and Zircon-Fission Track Thermochronology. *Tectonophysics* 751, 109–124. doi:10.1016/j.tecto.2018.12.005

Li, Q., Pan, B., Hu, X., Hu, Z., Li, F., and Yang, S. (2013). Apatite Fission Track Constraints on the Pattern of Faulting in the North Qilian Mountain. *J. Earth Sci.* 24 (4), 569–578. doi:10.1007/s12583-013-0350-1

Li, C., Zheng, D., Zhou, R., Wang, W., Yu, J., Liu, C., et al. (2021). Topographic Growth of the Northeastern Tibetan Plateau during the Middle-late Miocene: Insights from Integrated Provenance Analysis in the NE Qaidam Basin. *Basin Res.* 33 (6), 3212–3230. doi:10.1111/bre.12600

Lin, X., Chen, H., Wyrwoll, K.-H., Batt, G. E., Liao, L., and Xiao, J. (2011). The Uplift History of the Haiyuan-Liupan Shan Region Northeast of the Present Tibetan Plateau: Integrated Constraint from Stratigraphy and Thermochronology. *J. Geology.* 119 (4), 372–393. doi:10.1086/660190

Lin, X., Tian, Y., Donelick, R. A., Liu-Zeng, J., Cleber, S. J., Li, C. A., et al. (2019). Mesozoic and Cenozoic Tectonics of the Northeastern Edge of the Tibetan Plateau: Evidence from Modern River Detrital Apatite Fission-Track Age Constraints. *J. Asian Earth Sci.* 170, 84–95. doi:10.1016/j.jseaes.2018.10.028

Liu, Y., Genser, J., Neubauer, F., Jin, W., Ge, X., Handler, R., et al. (2005). 40Ar/39Ar mineral Ages from Basement Rocks in the Eastern Kunlun Mountains, NW China, and Their Tectonic Implications. *Tectonophysics* 398 (3-4), 199–224. doi:10.1016/j.tecto.2005.02.007

Liu, Y. J., Genser, J., Neubauer, F., Jin, W., Ge, X., and Handler, R. (2000). Geochronology of $^{40}Ar/^{39}Ar$ Dating in the Basement Rocks in Eastern Kunlun Mountains and its Tectonic Implications. *Earth Sci. Front.* 7 (Suppl. l), 227. doi:10.3321/j.issn:1005-2321.2000.z1.138

Lippert, P. C., van Hinsbergen, D. J., and Dupont-Nivet, G. (2014). Early Cretaceous to Present Latitude of the central Proto-Tibetan Plateau: A Paleomagnetic Synthesis with Implications for Cenozoic Tectonics, Paleogeography, and Climate of Asia. *Geol. Soc. America Spec. Pap.* 507, 1–21. doi:10.1130/2014.2507(01)

Malusà, M. G., and Fitzgerald, P. G. (2020). The Geologic Interpretation of the Detrital Thermochronology Record within a Stratigraphic Framework, with Examples from the European Alps, Taiwan and the Himalayas. *Earth-Science Rev.* 201, 103074. doi:10.1016/j.earscirev.2019.103074

Meng, Q. R., and Fang, X. (2008). "Cenozoic Tectonic Development of the Qaidam Basin in the Northeastern Tibetan Plateau,". *Investigations into the Tectonics of the Tibetan Plateau*. Editors B. C. Burchfiel and E. Wang (Boulder: Geological Society of America Special Paper), 444, 1–24. doi:10.1130/2008.2444(0110.1130/2008.2444(01)

Meng, Q., Song, C., Nie, J., Liu, C., He, P., Liu, F., et al. (2020). Middle-late Miocene Rapid Exhumation of the Southern Qilian Shan and Implications for Propagation of the Tibetan Plateau. *Tectonophysics* 774, 228279. doi:10.1016/j.tecto.2019.228279

Meyer, B., Tapponnier, P., Bourjot, L., Métivier, F., Gaudemer, Y., Peltzer, G., et al. (1998). Crustal Thickening in Gansu-Qinghai, Lithospheric Mantle Subduction, and Oblique, Strike-Slip Controlled Growth of the Tibet Plateau. *Geophys. J. Int.* 135 (1), 1–47. doi:10.1046/j.1365246X.1998.00567.x

Mock, C., Arnaud, N. O., and Cantagrel, J.-M. (1999). An Early Unroofing in Northeastern Tibet? Constraints from 40Ar/39Ar Thermochronology on Granitoids from the Eastern Kunlun Range (Qianghai, NW China). *Earth Planet. Sci. Lett.* 171 (1), 107–122. doi:10.1016/S0012-821X(99)00133-8

Molnar, P., and Stock, J. M. (2009). Slowing of India's Convergence with Eurasia since 20 Ma and its Implications for Tibetan Mantle Dynamics. *Tectonics* 28, a–n. doi:10.1029/2008TC002271

Murphy, M. A., Yin, A., Harrison, T. M., Dürr, S. B., Z, C., Ryerson, F. J., et al. (1997). Did the Indo-Asian Collision Alone Create the Tibetan Plateau?. *Geol* 25 (8), 719–722. doi:10.1130/0091-7613(1997)025<0719:dtiaca>2.3.co;2

Najman, Y., Henderson, A., Boudagherfadel, M., Godin, L., Parrish, R., Bown, P., et al. (2010). *Egu General Assembly Conference*. EGU General Assembly Conference Abstracts.The Sedimentary Record of India-Asia Collision: an Evaluation of New and Existing Constraints.

Pang, J., Yu, J., Zheng, D., Wang, W., Ma, Y., Wang, Y., et al. (2019a). Neogene Expansion of the Qilian Shan, North Tibet: Implications for the Dynamic Evolution of the Tibetan Plateau. *Tectonics* 38, 1018–1032. doi:10.1029/2018tc005258

Pang, J., Yu, J., Zheng, D., Wang, Y., Zhang, H., Li, C., et al. (2019b). Constraints of New Apatite Fission-Track Ages on the Tectonic Pattern and Geomorphic Development of the Northern Margin of the Tibetan Plateau. *J. Asian Earth Sci.* 181, 103909. doi:10.1016/j.jseaes.2019.103909

Pullen, A., Kapp, P., Gehrels, G. E., DeCelles, P. G., Brown, E. H., Fabijanic, J. M., et al. (2008). Gangdese Retroarc Thrust belt and Foreland basin Deposits in the Damxung Area, Southern Tibet. *J. Asian Earth Sci.* 33, 323–336. doi:10.1016/j.jseaes.2008.01.005

QBGM (1991). Qinghai Bureau of Geology and Mineral Resources. in *Geologic History of the Qinghai Province*. Beijing: Geological Publishing House.

Qi, B., Hu, D., Wang, J., Wang, X., Zhang, X., Zhang, Y., et al. (2013). ESR Dating of the Palaeogene in Muli Basin in the Middle of Qilian Mountains and its Geological Significance. *J. Geom.* 4, 392–402. [Chinese with English abstract].

Qi, B., Hu, D., Yang, X., Zhang, X., and Zhao, X. (2015). Paleoelevation of the Qilian Mountain Inferred from Carbon and Oxygen Isotopes of Cenozoic Strata. *Acta Geosci. Sin.* 36, 323–332. doi:10.3975/cagsb.2015.03.07

Qi, B., Hu, D., Yang, X., Zhang, Y., Tan, C., Zhang, P., et al. (2016). Apatite Fission Track Evidence for the Cretaceous-Cenozoic Cooling History of the Qilian Shan (NW China) and for Stepwise Northeastward Growth of the Northeastern Tibetan Plateau since Early Eocene. *J. Asian Earth Sci.* 124, 28–41. doi:10.1016/j.jseaes.2016.04.009

Ritts, B. D., and Biffi, U. (2000). Magnitude of post-Middle Jurassic (Bajocian) Displacement on the central Altyn Tagh Fault System, Northwest China. *Geol. Soc. America Bull.* 112 (1), 61–74. doi:10.1130/0016-7606(2000)112<61:mopjbd>2.0.co;2

Ritts, B. D., Yue, Y., and Graham, S. A. (2004). Oligocene-Miocene Tectonics and Sedimentation along the Altyn Tagh Fault, Northern Tibetan Plateau: Analysis of the Xorkol, Subei, and Aksay Basins. *J. Geology.* 112 (2), 207–229. doi:10.1086/381658

Rowley, D. B., and Currie, B. S. (2006). Palaeo-altimetry of the Late Eocene to Miocene Lunpola basin, central Tibet. *Nature* 439 (7077), 677–681. doi:10.1038/nature04506

Sobel, E. R., Arnaud, N., Jolivet, M., Ritts, B. D., and Brunel, M. (2001). "Jurassic to Cenozoic Exhumation History of the Altyn Tagh Range, Northwest China, Constrained by 40Ar/39Ar and Apatite Fission Track Thermochronology,".

Paleozoic and Mesozoic Tectonic Evolution of Central and Eastern Eurasia: From Continental Assembly to Intracontinental Deformation. Editors M. S. Hendrix and G. A. Davis, *Mem. Geol. Soc. Am.*, 194, 247–268. doi:10.1130/0-8137-1194-0.247

Sobel, E. R., and Seward, D. (2010). Influence of Etching Conditions on Apatite Fission-Track Etch Pit Diameter. *Chem. Geology*. 271, 59–69. doi:10.1016/j.chemgeo.2009.12.012

Spicer, R. A., Tao, Su., Valdes, P. J., Alexander, F., Wu, F-X., Shi., G., et al. (2020). Why the 'uplift of the Tibetan Plateau' Is a Myth. *Natl. Sci. Rev*. doi:10.1093/nsr/nwaa091

Staisch, L. M., Niemi, N. A., Clark, M. K., and Chang, H. (2016). Eocene to Late Oligocene History of Crustal Shortening within the Hoh Xil Basin and Implications for the Uplift History of the Northern Tibetan Plateau. *Tectonics* 35, 862–895. doi:10.1002/2015tc003972

Sundell, K. E., and Saylor, J. E. (2017). Unmixing Detrital Geochronology Age Distributions. *Geochem. Geophys. Geosyst.* 18, 2872–2886. doi:10.1002/2016GC006774

Tapponnier, P., Meyer, B., Avouac, J. P., Peltzer, G., Gaudemer, Y., Shunmin, G., et al. (1990). Active Thrusting and Folding in the Qilian Shan, and Decoupling between Upper Crust and Mantle in Northeastern Tibet. *Earth Planet. Sci. Lett.* 97, 382387–383403. doi:10.1016/0012-821x(90)90053-z

Tapponnier, P., Zhiqin, X., Roger, F., Meyer, B., Arnaud, N., Wittlinger, G., et al. (2001). Oblique Stepwise Rise and Growth of the Tibet Plateau. *Science* 294, 1671–1677. doi:10.1126/science.105978

Tian, Y., Kohn, B. P., Hu, S., and Gleadow, A. J. W. (2014). Postorogenic Rigid Behavior of the Eastern Songpan-Ganze Terrane: Insights from Low-Temperature Thermochronology and Implications for Intracontinental Deformation in central Asia. *Geochem. Geophys. Geosyst.* 15, 453–474. doi:10.1002/2013gc004951

Van der Beek, P., Robert, X., Mugnier, J.-L., Bernet, M., Huyghe, P., and Labrin, E. (2006). Late Miocene - Recent Exhumation of the central Himalaya and Recycling in the Foreland basin Assessed by Apatite Fission-Track Thermochronology of Siwalik Sediments, Nepal. *Basin Res.* 18 (4), 413–434. doi:10.1111/j.1365-2117.2006.00305.x

Vermeesch, P. (2012). On the Visualisation of Detrital Age Distributions. *Chem. Geology*. 312-313, 190–194. doi:10.1016/j.chemgeo.2012.04.021

Vincent, S. J., and Allen, M. B. (1999). Evolution of the Minle & Chao Shui Basins, china: Implications for Mesozoic Strike-Slip basin. *Geol. Soc. America Bull.* 111, 725–742. doi:10.1029/2019TC005705

Wan, J., Zheng, W., Zheng, D., Wang, W., and Wang, Z. (2010). Low Closure Temperature Thermochronometry Study on the Late Cenozoic Tectonic Active of Northern Qilianshan and its Implication for Dynamics of Tibetan Plateau Growth. *Geochimica* 39 (5), 439–446. doi:10.1017/S0004972710001772

Wang, W., Zheng, D., Li, C., Wang, Y., Zhang, Z., Pang, J., et al. (2020). Cenozoic Exhumation of the Qilian Shan in the Northeastern Tibetan Plateau: Evidence from Low-Temperature Thermochronology. *Tectonics* 39. doi:10.1029/2019TC005705

Wang, W., Zheng, W., Zhang, P., Li, Q., Kirby, E., Yuan, D., et al. (2017). Expansion of the Tibetan Plateau during the Neogene. *Nat. Commun.* 8, 15887. doi:10.1038/ncomms15887

Wang, X., Song, C., Zattin, M., He, P., Song, A., Li, J., et al. (2016). Cenozoic Pulsed Deformation History of Northeastern Tibetan Plateau Reconstructed from Fission-Track Thermochronology. *Tectonophysics* 672-673, 212–227. doi:10.1016/j.tecto.2016.02.006

Wang, Y., Zheng, J., Zheng, Y., Liu, X., and Sun, G. (2015a). Paleocene-Early Eocene Uplift of the Altyn Tagh Mountain: Evidence from Detrital Zircon Fission Track Analysis and Seismic Sections in the Northwestern Qaidam basin. *J. Geophys. Res. Solid Earth* 120 (12), 8534–8550. doi:10.1002/2015jb011922

Wang, Y., Zhang, J., Qi, W., and Guo, S. (2015b). Exhumation History of the Xining Basin since the Mesozoic and its Tectonic Significance. *Acta Geologica Sinica - English Edition* 89 (1), 145–162. doi:10.1111/1755-6724.12401

Wang, C., Zhao, X., Liu, Z., Lippert, P. C., Graham, S. A., Coe, R. S., et al. (2008). Constraints on the Early Uplift History of the Tibetan Plateau. *Pnas* 105 (13), 4987–4992. doi:10.1073/pnas.0703595105

Xiao, G., Guo, Z., Dupont-Nivet, G., Lu, H., Wu, N., Ge, J., et al. (2012). Evidence for Northeastern Tibetan Plateau Uplift between 25 and 20Ma in the Sedimentary Archive of the Xining Basin, Northwestern China. *Earth Planet. Sci. Lett.* 317-318, 185–195. doi:10.1016/j.epsl.2011.11.008

Yang, R., Fang, X., Meng, Q., Zan, J., Zhang, W., Deng, T., et al. (2017). Paleomagnetic Constraints on the Middle Miocene-Early Pliocene Stratigraphy in the Xining Basin, NE Tibetan Plateau, and the Geologic Implications. *Geochem. Geophys. Geosyst.* 18, 3741–3757. doi:10.1002/2017gc006945

Yin, A., Dang, Y.-Q., Wang, L.-C., Jiang, W.-M., Zhou, S.-P., Chen, X.-H., et al. (2008). Cenozoic Tectonic Evolution of Qaidam basin and its Surrounding Regions (Part 1): The Southern Qilian Shan-Nan Shan Thrust belt and Northern Qaidam basin. *Geol. Soc. America Bull.* 120, 813–846. doi:10.1130/b26180.1

Yin, A., and Harrison, T. M. (2000). Geologic Evolution of the Himalayan-Tibetan Orogen. *Annu. Rev. Earth Planet. Sci.* 28, 211–280. doi:10.1146/annurev.earth.28.1.211

Yin, A., Rumelhart, P. E., Butler, R., Cowgill, E., Harrison, T. M., Foster, D. A., et al. (2002). Tectonic History of the Altyn Tagh Fault System in Northern Tibet Inferred from Cenozoic Sedimentation. *Geol. Soc. America Bull.* 114, 1257–1295. doi:10.1130/0016-7606(2002)114<1257:thotat>2.0.co;2

Yu, J. X., Pang, J. Z., Wang, Y. Z., Zheng, D. W., Liu, C. C., Wang, W. T., et al. (2019). Mid-Miocene uplift of the northern Qilian Shan as a result of the northward growth of the northern Tibetan Plateau: *Geo*. 15 (2), 423–432. doi:10.1130/GES01520.1

Yu, X., Guo, Z., Zhang, Q., Cheng, X., Du, W., Wang, Z., et al. (2017). Denan Depression Controlled by Northeast-Directed Olongbulak Thrust Zone in Northeastern Qaidam basin: Implications for Growth of Northern Tibetan Plateau. *Tectonophysics* 717, 116–126. doi:10.1016/j.tecto.2017.06.017

Yuan, D.-Y., Champagnac, J.-D., Ge, W.-P., Molnar, P., Zhang, P.-Z., Zheng, W.-J., et al. (2011). Late Quaternary Right-Lateral Slip Rates of Faults Adjacent to the lake Qinghai, Northeastern Margin of the Tibetan Plateau. *Geol. Soc. America Bull.* 123 (9-10), 2016–2030. doi:10.1130/B30315.1

Yuan, D. Y., Ge, W. P., Chen, Z. W., Li, C. Y., Wang, Z. C., Zhang, H. P., et al. (2013). The Growth of Northeastern Tibet and its Relevance to Large-scale continental Geodynamics: A Review of Recent Studies. *Tectonics* 32 (5), 1358–1370. doi:10.1002/tect.20081

Yue, L., Heller, F., Qiu, Z., Zhang, L., Xie, G., Qiu, Z., et al. (2000). Paleomagnetic Age of the Tertiary Strata and Paleoenvironment Records in the Lanzhou basin [in Chinese with English Abstract]. *Chin. Sci. Bull.* 45 (18), 1998–2003.

Zhang, J., Wang, Y., Zhang, B., and Zhang, Y. (2016). Tectonics of the Xining Basin in NW China and its Implications for the Evolution of the NE Qinghai-Tibetan Plateau. *Basin Res.* 28, 159–182. doi:10.1111/bre.12104

Zhang, T., Fang, X., Wang, Y., Song, C., Zhang, W., Yan, M., et al. (2018). Late Cenozoic Tectonic Activity of the Altyn Tagh Range: Constraints from Sedimentary Records from the Western Qaidam Basin, NE Tibetan Plateau. *Tectonophysics* 737, 40–56. doi:10.1016/j.tecto.2018.04.021

Zhang, W., Fang, X., Zhang, T., Song, C., Yan, M., et al. (2020). Eocene Rotation of the Northeastern Central Tibetan Plateau Indicating Stepwise Compressions and Eastward Extrusions. *Geophys. Res. Lett.* 47 (17), e2020GL088989. doi:10.1029/2020GL088989

Zhang, T., Han, W., Fang, X., Song, C., Wang, Y., Tian, Q., et al. (2021). Tectonic Forcing of Environmental Transition in Central Asia at ~11-9 Ma. *Gondwana Res.* 89, 19–30. doi:10.1016/j.gr.2020.08.012

Zhang, W. L., Zhang, T., Song, C. H., Appel, E., Mao, Z., Fang, Y., et al. (2017). Termination of Fluvial-Alluvial Sedimentation in the Xining Basin, NE Tibetan Plateau, and its Subsequent Geomorphic Evolution Plio-Quaternary Terrace Development in the Xining Basin, NE Tibetan Plateau. *Geomorphology* 297, 86–99. doi:10.1016/j.geomorph.2017.09.008

Zheng, D., Clark, M. K., Zhang, P., Zheng, W., and Farley, K. A. (2010). Erosion, Fault Initiation and Topographic Growth of the North Qilian Shan (Northern Tibetan Plateau). *Geosphere6* 6, 937–941. doi:10.1130/GES00523.1

Zheng, D., Wang, W., Wan, J., Yuan, D., Liu, C., Zheng, W., et al. (2017). Progressive Northward Growth of the Northern Qilian Shan-Hexi Corridor (Northeastern Tibet) during the Cenozoic. *Lithosphere* 9, 408–416. doi:10.1130/L587.1

Zhuang, G., Hourigan, J. K., Ritts, B. D., and Kent-Corson, M. L. (2011). Cenozoic Multiple-phase Tectonic Evolution of the Northern Tibetan Plateau: Constraints from Sedimentary Records from Qaidam basin, Hexi Corridor, and Subei basin, Northwest China. *Am. J. Sci.* 311, 116–152. doi:10.2475/02.2011.02

Zhuang, G., Johnstone, S. A., Hourigan, J., Ritts, B., Robinson, A., Sobel, E. R., et al. (2018). Understanding the Geologic Evolution of Northern Tibetan Plateau with Multiple Thermochronometers. *Gondwana Res.* 58, 195–210. doi:10.1016/j.gr.2018.02.014

Zhuang, G., Zhang, Y. G., Hourigan, J., Ritts, B., Hren, M., Hou, M., et al. (2019). Microbial and Geochronologic Constraints on the Neogene Paleotopography of Northern Tibetan Plateau. *Geophys. Res. Lett.* 46 (3), 1312–1319. doi:10.1029/2018gl081505

Zuza, A. V., Cheng, X., and Yin, A. (2016). Testing Models of Tibetan Plateau Formation with Cenozoic Shortening Estimates across the Qilian Shan-Nan Shan Thrust belt. *Geosphere* 12 (2), 501–532. doi:10.1130/ges01254.1

Zuza, A. V., Wu, C., Reith, R. C., Yin, A., Li, J., Zhang, J., et al. (2018). Tectonic Evolution of the Qilian Shan: An Early Paleozoic Orogen Reactivated in the Cenozoic. *Geol. Soc. America Bull.* 130, 881–925. doi:10.1130/B31721.1

Conflict of Interest: The authors declare that the research was conducted in the absence of any commercial or financial relationships that could be construed as a potential conflict of interest.

Publisher's Note: All claims expressed in this article are solely those of the authors and do not necessarily represent those of their affiliated organizations, or those of the publisher, the editors, and the reviewers. Any product that may be evaluated in this article, or claim that may be made by its manufacturer, is not guaranteed or endorsed by the publisher.